Measurement Report: Aircraft Observations of Ozone, Nitrogen Oxides, and Volatile Organic Compounds over Hebei Province, China

Sarah E. Benish[1], Hao He[1], Xinrong Ren[1,2], Sandra J. Roberts[3], Ross J. Salawitch[1,3], Zhanqing Li[1,4], Fei Wang[4,5], Yuying Wang[6], Fang Zhang[4], Min Shao[7], Sihua Lu[7], Russell R. Dickerson[1]

[1] Department of Atmospheric and Oceanic Science, University of Maryland, College Park, MD 20742, USA.
[2] Air Resources Laboratory, National Oceanic and Atmospheric Administration, College Park, MD 20740, USA.
[3] Department of Chemistry and Biochemistry, University of Maryland, College Park, MD 20742, USA.
[4] State Key Laboratory of Earth Surface Processes and Resource Ecology, College of Global Change and Earth System Science, Beijing Normal University, Beijing, 100875, China.
[5] Key Laboratory for Cloud Physics, Chinese Academy of Meteorological Sciences, Beijing, 100081, China.
[6] Key Laboratory for Aerosol-Cloud-Precipitation of China Meteorological Administration, School of Atmospheric Physics, Nanjing University of Information Science and Technology, Nanjing, 21004, China.
[7] College of Environmental Science and Engineering, Peking University, Beijing, 100871, China.

Correspondence to: Sarah E. Benish (sebenish@umd.edu)

Abstract. To provide insight into the planetary boundary layer (PBL) production of ozone (O_3) over the North China Plain, the Air chemistry Research in Asia (ARIAs) campaign conducted aircraft measurements of air pollutants over Hebei Province, China between May and June 2016. We evaluate vertical profiles of trace gas species including O_3, nitrogen oxides (NO_x), carbon monoxide (CO), and volatile organic compounds (VOCs) and relate to rates of O_3 production. This analysis shows measured O_3 levels ranged from 52 to 142 ppbv, with the peak median concentration (~94 ppbv) occurring between 1000 and 1500 m. The NO_x concentrations exhibited strong spatial and altitudinal variations, ranging from 0.15 to 49 ppbv. Ratios of CO/NO_y and CO/CO_2 indicate the prevalence of low efficiency combustion from biomass burning and residential coal burning. Concentrations of total measured VOCs from 26 whole air canisters reveals alkanes dominate the total measured volume mixing ratio of VOCs (68%) and we see evidence of vehicular emissions, fuel and solvent evaporation, and biomass burning sources. Alkanes and alkenes/alkynes are responsible for 74% of the total VOC reactivity assessed by calculating the OH loss rates, while aromatics contribute the most to the total Ozone Formation Potential (OFP) (43%) with toluene, m/p-xylene, ethylene, propylene, and i-pentane playing significant roles in the aloft production of O_3 in this region. In the PBL below 500 m, box model calculations constrained by measured precursors indicate the peak rate of mean O_3 production was ~7 ppbv/hour. Pollution frequently extended above the PBL into the lower free troposphere around 3000 m, where NO_2 mixing ratios (~400 pptv) led to net production rates of O_3 up to ~3 ppbv/hour; this pollution can travel substantial distances downwind. The O_3 sensitivity regime is determined to be NO_x-limited throughout the PBL, while more VOC-limited at low altitudes near urban centres, demonstrating both VOCs and NO_x need further control to reduce aloft O_3 over Hebei.

1 Introduction

Explosive urbanization and rapid industrialization contributed to high ground-level ozone (O_3) and particulate matter (PM) over the past several decades in the North China Plain (NCP) (Johnson et al., 2006; Ran et al., 2011; Shao et al., 2009; Zhang et al., 2014). Household burning of coal used for cooking and heating, emissions from gasoline, diesel, and liquified petroleum gas (LPG) vehicles, as well as large-scale burning of winter wheat residues in the NCP are some of the many sources responsible for O_3 precursors, such as nitrogen oxides (NO_x=NO+NO_2) and volatile organic compounds (VOCs) (Chen et al., 2017; Long et al., 2016; Stavrakou et al., 2016). Ozone is harmful to both the human respiratory system (Bell et al., 2006;

40   Jerrett et al., 2009) and to photosynthetic processes by vegetation (Avnery et al., 2011; Reich and Amundson, 1985), while some VOCs, such as benzene and chloroform, are known to be hemotoxic and carcinogenic (Environmental Protection Agency - Integrated Risk Information System, 2003; Lan et al., 2004). Several studies using the NASA Ozone Monitoring Instrument (OMI) have found reductions of some pollutants like sulfur dioxide (SO_2) over the NCP (He et al., 2012; Krotkov et al., 2016; Li et al., 2010, 2017), but NO_2 pollution still remains severe in China (Figure 1a).

45   Ozone is created through the oxidation of NO by hydroperoxyl radicals (HO_2) and organic peroxy radicals (RO_2), products of carbon monoxide (CO) and VOC oxidation. When one of these precursors is the limiting reactant, the rate of O_3 production is considered VOC- or NO_x-sensitive (Finlayson-Pitts and Pitts, 1999; Sillman et al., 1990). The role of VOCs on the formation of O_3 depends on the characteristics of the environment, including the main emission sources of primary pollutants and ambient temperature (Pusede et al., 2014). Quantifying the abundance of NO_x and the suite of VOC chemicals throughout the lower

50   troposphere is urgently needed to better understand the photochemistry of O_3 production in the NCP to develop successful mitigation strategies.

In-situ airborne measurements provide valuable information regarding the horizontal and vertical distributions of air pollutants over a large spatial area. Airborne measurements are necessary to characterize air pollution over large cities, as well as surrounding areas. Ozone and PM are produced throughout the planetary boundary layer (PBL), so aircraft observations can

55   lead to a more complete picture of pollution formation and transport than is available only from surface observations. While several airborne campaigns have deployed to investigate the regionally transported pollution problem in East Asia, including the NASA Korea-United States Air Quality Study (KORUS-AQ) (Al-Saadi et al., (2015), see https://www-air.larc.nasa.gov/missions/korus-aq/docs/White_paper_NASA_KORUS-AQ.pdf), that occurred at the same time as our measurements, few airborne studies characterize the source region of severe smog within the Hebei Province region of China.

60   Through Chinese/American partnerships with Peking University, Beijing Normal University, and the University of Maryland, we conducted a field campaign in Hebei Province, China called Air chemistry Research In Asia (ARIAs). The Ministry of Environmental Protection of the People's Republic of China reported six of the top ten cities with the worst air quality in 2016 were located in Hebei (including the capital city of Shijiazhuang), illustrating the need for more research characterizing air pollution in this region. In this study, we analyse concentrations of O_3, NO_x, NO_y, CO, and VOCs obtained during 11 research

65   flights between May and June 2016. The VOC chemical reactivity and impact on O_3 production is assessed and we utilize an observation-constrained box model to evaluate photochemical properties of the production of O_3 that occurs throughout the lower free troposphere.

2 Materials and Methods

2.1 Air sampling and analysis

70   The ARIAs campaign included 11 research flights from May-June 2016 in Hebei Province (Fig. 1b). Flight days were chosen based on meteorological conditions associated with smog events, such as higher temperatures, little cloud cover, low relative

Atmospheric
Chemistry
and Physics
Discussions
Open Access
EGU

humidity, weak winds, and shallow PBL height (Tang et al., 2012). The Y-12 aircraft was based at Luancheng Airport (114.59°E, 37.91°N, 58 m above sea level (ASL)), located in southeast Shijiazhuang (population around 10 million), a major economic centre in Hebei, including pharmaceutical and textile industries, machinery and chemical manufacturing, construction, and electronics production. Flight sampling occurred east of the Taihang Mountains and the Y-12 flew vertical spirals from ~300 m to ~3500 m over Shijiazhuang as well as three other locations: Julu (115.02°E, 37.22°N, 30 m ASL), Quzhou (114.96°E, 36.76°N, 40 m ASL), and Xingtai (114.36°E, 37.18°N, 182 m ASL) (see Table S1 for a description of flight paths, weather conditions, and statistics of measured trace gases).

Various instruments aboard the Y-12 aircraft collected trace gas, aerosol, and meteorological data. The aircraft instrumentation (Table 1) included different gas and particle sample inlets on the top of the fuselage and pressure/temperature/humidity sensors (Cloud Water Inertial Probe (CWIP), Rain Dynamics) installed under one wing of the aircraft (Fig. S1). Flight position data were recorded using a portable global positioning system (GPS) and the CWIP. The aircraft was equipped with the following trace gas analysers: (1) a Picarro cavity ring down spectrometer (CRDS) for measurements of CH_4, CO_2, CO, and H_2O; (2) a Thermal Electron Corporation (TECO) Model 49C UV absorption O_3 analyser; (3) a TECO Model 43C pulsed fluorescence SO_2 analyser; (4) a Los Gatos Research Model RMT-200 CRDS NO_2 analyser; and (5) a TECO Model 42C NO-NO_y analyser. Power constraints and a converter issue led to limited NO_y, NO_x, and CO measurements during the campaign, particularly in the lower free troposphere (LFT). Negative values indicate readings around the detection limit, usually at high altitudes. The aircraft was also equipped with an inlet to measure aerosols up to ~5.0 μm diameter and aerosol optical properties, including a nephelometer (TSI Model 3563) to measure aerosol scattering, a particle soot absorption photometer (PSAP) to measure aerosol absorption, and an aethalometer (Magee Model AE31) and a Single-Particle Soot Photometer (SP2, Droplet Measurement Technologies) to measure black carbon. Observed aerosol optical properties have been summarized by F. Wang et al. (2018); further details on aircraft instrumentation are given by Ren et al. (2018).

Twenty-six whole air samples (WAS) were collected directly into 3.2 L fused silica lined electropolished stainless steel canisters (Entech Instrument Inc., Simi Valley, CA) at a variety of pressure altitudes from 400 m to 3500 m between 1:30 and 9:00 UTC (9:30 and 17:00 local time). The sampling period for the WAS canisters was approximately 1-2 minutes during the spirals. Samples were analysed for 54 VOCs and 22 halocarbons. Since the halogenated species have negligible effects on O_3 production, we exclude these species from the analysis presented here. We also exclude 2 WAS canisters from this analysis due to evidence of contamination after collection (Text S1). Limited samples collected over one province in one season may not be able to represent O_3 chemistry for all of China, but the scarcity of airborne VOC measurements in this region makes these data valuable for characterizing the composition of air throughout and above the PBL, demonstrating how the production of O_3 aloft differs from that at the surface.

The VOC analytical techniques used by the College of Environmental Sciences and Engineering at Peking University (PKU) in Beijing have been summarized in the past (Mo et al., 2015; Wang et al., 2010a), and we briefly describe the method here. The WAS canisters were cleaned following a standard sampling procedure, pressured with nitrogen and vacuumed three times to 2.6 Pa. The hydrocarbons were quantified using a gas chromatograph equipped with a mass selective detector (GC-MSD,

Hewlett Packard 5975/7890, USA) and a flame ionization detector (FID) coupled with a cryofocusing pre-concentration system (Entech Instrument 7100A, Simi Valley, CA). This system used a Dean Switch™ (Agilent Technologies, Santa Clara, CA, USA) to introduce the effluent into a DB-624 column (60 m × 0.25 mm × 1.8 μm; J&W Scientific, Folsom, CA, USA) with an MSD to separate and analyse C4–C12 hydrocarbons and halocarbons. A PLOT (Al/KCl) column (30 m × 0.25 mm × 3.0

110 μm; J&W Scientific) with an FID was used to measure the C2–C4 hydrocarbons.

The Photochemical Assessment Monitoring Stations (PAMS) (55 NMHCs) and Toxic Organic-15 (TO-15) standard mixtures were used to calibrate the GC-MSD/FID system that measured the C2–C12 VOCs. Samples with known concentrations of four VOCs (bromochloromethane, 1,4-difluorobenzene, chlorobenzene-d5 and 1-bromo-3-fluorobenzene) were used as internal standards for each sample to calibrate the system. The GC-MSD/FID system was calibrated at five concentrations,

115 ranging from 0.5 to 8 ppbv, for each of these four compounds before sample analysis. Correlation coefficients, ranging from 0.987 to 0.999 showed that the integral areas of peaks were proportional to the concentrations of the target compounds. A gas standard (diluting from 1 ppmv to 2 ppbv) was measured each day to check the stability of the system. Summary statistics of the VOCs along with the method detection limit (MDL) (ranging from 0.002 to 0.027 ppbv) are reported in Table S2. Total uncertainty for VOC measurements reflects instrument noise, plus uncertainty in calibration standards, contamination, and

120 pressurization. Best estimate of the total uncertainty is ±20% with 95% confidence due to uncertainties associated with airborne sampling platforms. Intercomparison experiments of VOC measurements between PKU and other laboratories showed good agreement (Liu et al., 2008b).

The Atmosphere-Aerosol-Boundary Layer-Cloud (A²BC) Interaction Joint Experiment campaign collected meteorological, aerosol, and trace gas information from a ground-based site in Xingtai (114.36°E, 37.18°N, 182 m ASL) from May to

125 December 2016 (Wang et al., 2018b, 2019). An intensive observation period in May and June 2016 was conducted to coincide with ARIAs. Data from A²BC instruments used in our analysis include: (1) a NO_x analyser with a molybdenum converter (Ecotech model 9841A); (2) an infrared absorption CO analyser (Ecotech model 9830A); and (3) a UV absorption O_3 analyser (Ecotech model 9810A). Results of NO_2, SO_2, HONO, HCHO, CHOCHO, and aerosols derived from the Differential Optical Absorption Spectrometer (DOAS) are summarized by Yang Wang et al., (2019). The A²BC site is located in northwest Xingtai,

130 nestled in the east foothill of the Taihang Mountains. Agricultural crops surround the site, consisting heavily of winter wheat, that is harvested, with the stubble burned in June (Liu and Si, 2011). Xingtai is a city with approximately 7 million people and is surrounded by industry including coal mining and coal-burning power plants, cement and steel industries, chemical processing, iron-smelting, and glass manufacturing.

2.2 Box Model Simulations

135 A box model called Framework in 0-Dimensional Atmospheric Modelling (F0AMv3.1) (Wolfe et al., 2016) is used to evaluate oxidation processes to understand O_3 photochemical production both at the surface and aloft. The box model simulations cover the Y-12 flight tracks during seven flights and daytime hours at the A²BC supersite in Xingtai (where the Y-12 conducted spirals) using the Carbon Bond Mechanism, version 6, revision 2 (CB6r2). The model is constrained by observed

Atmospheric
Chemistry
and Physics
Discussions

Open Access

EGU

concentrations of VOCs, NO_2, CO, and O_3. Periodic missing Y-12 NO_2 data due to internal auto-zeroing are linearly
140   interpolated since gaps were short (~2 minutes). A physical loss lifetime is set to 24 hours to mitigate build-up of long-lived
oxidation products over multiple days of integration. Ground observations are only used for days that a flight occurred. For
May 17, surface data for NO_2 is filled with 1-hour average data collected for other days of the month, due to missing surface
measurements on this day. For every 5-minute interval of ground data, the model is run with a 1-hour time step for 3 days with
changing solar zenith angle calculated for the location of ground observations. For each 1-minute interval of flight data, the
145   model is run with a 1-hour time step for 5 days in "solar cycle" mode, allowing photolysis frequencies to evolve over the
course of a model step and for calculated reactive intermediates to achieve diel steady state. Photolysis frequencies (not
measured during ARIAs) are calculated by combining cross sections and quantum yields with solar spectra derived from the
NCAR Tropospheric Ultraviolet and Visible (TUV) version 5.2 radiation model. At the start of the model run, input solar
zenith angle, altitude, O_3 column, and surface albedo are used for linear interpolation across TUV lookup tables (F0AM's
150   "hybrid" method). A correction factor is used to scale j-values to better agree with the observed NO/NO_2 ratio. Optical depth,
single scattering albedo, and angstrom exponent during ARIAs (see Wang et al., (2018a)) are used in the TUV online calculator
(https://cprm.acom.ucar.edu/Models/TUV/Interactive_TUV/) to assess the impact of aerosols on photolysis frequencies. The
impact of aerosol optical properties measured during ARIAs on photolysis frequencies is small compared to the default setting,
so no additional adjustments are made to the model.

155   Due to the limited number of grab canisters per flight, VOCs are constrained based on the altitude of the sampling relative to
the height of the PBL, which is determined using potential temperature and water vapor vertical profiles for each flight. All
WAS canisters collected below the top of the PBL during a flight are averaged. All of the WAS canisters for the entire
campaign collected above the research flight's PBL are averaged for that flight. The average concentration of the samples
below 500 m is used as ground concentrations since A^2BC did not measure VOCs at the surface. This method to constrain
160   VOCs introduces large uncertainty due to the sparsity of measurements obtained over a large area that potentially consists of
a wide variety of chemical compositions. However, the production of O_3 aloft is not well characterized over Hebei, so our
observations may help improve the understanding of air pollution for this region, despite this limitation.

Unlike a 3-dimensional chemical transport model, the box model simulations do not include advection or emissions. These
processes, while important, are not included in the box model since O_3 precursors were measured and used to constrain the
165   model calculations. Box modelling is used to gain an understanding of O_3 production and its sensitivity to ambient levels of
NO_x and VOCs based upon measured meteorological parameters and the concentration of a wide variety of chemical species.

2.2.1 Ozone Production and Sensitivity Calculations

The photochemical production of O_3 during the daytime is determined by the production rate of NO_2 molecules from the
HO_2+NO and RO_2+NO reactions minus the loss mechanisms (Finlayson-Pitts and Pitts, 1999). Thus, the net O_3 production
170   rate, net(PO_3) can be estimated following Equation 1:

$$net(PO_3) = k_{HO_2+NO}[HO_2][NO] + \sum_{i=1}^{n} k_{RO_{2i}+NO}[RO_{2i}][NO] - P(RONO_2)$$

$$-k_{OH+NO_2+M}[OH][NO_2][M] - k_{HO_2+O_3}[HO_2][O_3] - k_{OH+O_3}[OH][O_3]$$
$$-k_{O(^1D)+H_2O}[O(^1D)][H_2O] - L(O_3 + alkenes) \tag{1}$$

where k denotes the different reaction rate constants and RO_{2i} is the concentration of individual organic perxoy radicals. The terms subtracted from the production of O_3 are the loss mechanisms: the formation of nitrates, $P(RONO_2)$, the reaction of OH and NO_2 to form nitric acid, the reactions of OH and HO_2 with O_3, the reaction of $O(^1D)$ with H_2O, and the reactions of O_3 with alkenes. Additional terms not included here are the rate of O_3 loss by dry deposition and direct loss on aerosol surfaces (dilution is the only physical loss in the current F0AM setup).

We evaluate the sensitivity of O_3 production to NO_x and VOCs using the ratio of L_N/Q, where L_N is the radical loss through reactions with NO and Q is the primary radical production (Kleinman, 2005a). When L_N/Q is much less than 0.5, the O_3 production regime is NO_x-limited; when L_N/Q ratio is much higher than 0.5, the regime is VOC-limited. Different environments can have varying amounts of organic nitrates that impact the cut-off value of L_N/Q, so this value could vary around 0.5 (Kleinman, 2005b).

3 Results and discussion

3.1 Observations of nitrogen oxides, carbon monoxide, and ozone

Our observations confirm heavy loadings of air pollution over Hebei. Vertical profiles show peak median concentrations of NO (1.6 ppbv), NO_2 (4.4 ppbv) and NO_y (25.7 ppbv) below 500 m with large variability (Fig. 2). Median concentrations of NO and NO_2 drop off gradually with altitude, while median NO_y remains close to ~15 ppbv throughout most of the profile. Between 500 and 1000 m, sufficient levels of NO_x are observed (median=3.8 ppbv), indicating continued production of O_3 in the PBL. Above 3000 m, median concentrations of NO and NO_2 fall to 350 pptv and 106 pptv, respectively (not measured simultaneously), still sufficient to produce O_3 as air parcels travels downwind. Median mixing ratios of O_3 and CO remain high (~80 ppbv and ~120 ppbv, respectively) throughout the altitudes sampled by the Y-12.

Unlike previous airborne studies over Beijing from 1994-2005 that found increased O_3 concentrations below 1 km with constant levels (~52 ppbv) between 1 and 2 km (Ding et al., 2008), our O_3 concentrations peaked between 1000 and 1500 m (median = 91.6 ppbv). Low ratios of NO_x/NO_y (<0.30) indicate significant O_3 production had already occurred, but the strong correlation (R=0.77, Fig. S2) between 1-minute NO_z (NO_y-NO_x) and O_x (O_3+NO_2), an empirical estimate of the O_3 production efficiency (OPE), below 1500 m demonstrates moderate production of O_3 continued during sampling. The OPE of ~4 during ARIAs is smaller than the average OPE value of ~8 obtained during 2013 DISCOVER-AQ flights in Houston (Mazzuca et al., 2016), likely due to the higher NO_x concentrations observed in Hebei than Texas.

Atmospheric
Chemistry
and Physics
Discussions

Maps of O_3 and NO_2 on the Y-12 flight tracks (Fig. 3) show the largest concentrations around the spiral locations as well as
200 between the three most northern cities, Shijiazhuang, Julu, and Xingtai. Regions of elevated NO_2 do not always correspond
with high O_3 concentrations. The flight with the maximum observed NO_2 mixing ratio (35.3 ppbv) during ARIAs occurred on
May 17 around 8:30 am LST. The aircraft was flying a flat transect at 500 m from Shijiazhuang to Julu when a large peak of
NO_2, CO_2 (500 ppmv), and NO (15 ppbv) was sampled. Concentrations of O_3 were low during the time of the peak (~60 ppbv),
indicating NO-O_3 titration, but O_3 levels were quite high (>90 ppbv) throughout the remainder of the flight. The maximum O_3
205 concentration (142.5 ppbv) was measured on May 21 during descent into Luancheng Airport in Shijiazhuang. Observations of
NO_x were not available for this flight, but elevated CO concentrations (565 ppbv) were observed. High concentrations of O_3
were also observed away from the large megacities. For instance, an O_3 plume (~125 ppbv) was sampled on June 6 at 1500 m
over a more suburban area between Shijiazhuang and Julu with NO_2 levels ~500 pptv.

Vertical profiles of trace gases over the four spiral locations (Fig. 4) generally show the highest concentrations over the two
210 largest cities, Shijiazhuang and Xingtai. These two megacities exhibit the greatest variability, below 500 m altitude, of all
trace gases discussed here below 500 m. At 3000 m, Xingtai demonstrates the most NO_2 (~800 pptv), while the other spiral
locations show ~300 pptv. Median profiles of NO_y below 500 m are highest over Julu (27.6 ppbv), while aloft concentrations
are similar between the spiral locations (~13 ppbv between 2500-3000 m). Median vertical profiles of CO are relatively
consistent (~300 ppbv) below 2000 m over the spiral locations, while Julu shows the highest median concentrations between
215 2500 and 3000 m (194.1 ppbv). Measurements of CO above Xingtai indicate a large spread in observations at all altitudes from
the lowest 500 m (10th percentile= 258 ppbv, 90th percentile=1049 ppbv) up to 2000 m (10th percentile=97.7 ppbv, 90th
percentile = 135 ppbv). This variability may be partially explained by the possible burning of wheat straw during early summer
2016. Strong correlations between ethane and acetylene, two biomass burning markers (see Section 3.2), further suggest wheat
residue burning over Xingtai. Median vertical profiles of O_3 below 500 m were 10-25 ppbv higher in Shijiazhuang
220 (median=96.2 ppbv) than the other spiral locations. Concentrations of O_3 are generally stable or slightly increasing in the
lowest 2000 m, and median O_3 is 75-80 ppbv even as high as 2500-3000 m. Xingtai shows the smallest variability of aloft O_3
levels above 2000 m, likely due to the position of this city on the leeward side of the Taihang Mountains.

The overall measured concentrations (1-minute average, standard deviation, minimum, and maximum values) of NO_x, CO,
and O_3 in this study are compared with other airborne studies in China including KORUS-AQ flights when outflow was directly
225 from China (Table 2). Comparable to our range of NO_x levels from 0.15 to 49.3 ppbv, autumn flights in the Yangtze River
Delta in 2007 documented large variability in NO_x concentrations, ranging from 3 to 40 ppbv (Geng et al., 2009), while April
2006 observations in northern China similarly find a mean concentration ~5 ppbv (Wang et al., 2008). The minimum CO
concentration during ARIAs (90.6 ppbv) was measured in the lower free troposphere, which is a much smaller minimum
concentration than reported by earlier studies. The warm-sector PBL air ahead of a cold front in April 2007 in Shenyang
230 Province in northeast China found ~300 ppbv CO between 1000 and 4000 m (Dickerson et al., 2007), generally larger than
most ARIAs profiles (except for Julu). The maximum value of CO during ARIAs (almost 2 ppmv) agrees better with the
literature, although there are few reported aircraft measurements of CO in Northeast Asia. Average and maximum O_3

concentrations during ARIAs were much higher than in other studies, but comparable to KORUS-AQ measurements from
May 24-29 when the flow of air was direct from China. Since the majority of past airborne studies occurred over the sea areas
235 during other seasons, it is not surprising that an urbanized environment like Hebei experienced much larger amounts of O_3
than previously reported.

The ratios between combustion tracers can be used to understand the source and efficiency. During high-efficiency combustion
in modern power plants, fuel carbon is converted to CO_2 with near unit efficiency, resulting in low CO/CO_2 (<0.10%), while
low-efficiency combustion (cold or smoldering processes or low-technology combustion) yields larger ratios. The regression
240 of 1-minute CO against CO_2 (Fig. 5a) shows high linear correlation (R=0.90) and high ratios of CO/CO_2 (2.4%) together with
large amounts of SO_2. These measurements are indicative of low-efficiency fossil fuel combustion, likely from residential coal
burning as these observations were all collected at ~500 m. These results agree with airborne data from the KORUS-AQ
campaign during Chinese-sourced inflow indicating 1-4% CO/CO_2 (attributing to low-efficiency combustion) (Halliday et al.,
2019). Similarly, Xia et al. (2020) found higher CO/CO_2 ratios ~2% in December 2017 at Jingdezhen station in central China
245 when air mass transport was from northern China, although they note some high combustion efficiency may be found in Jiangxi
and Hunan provinces in Central China. Higher CO/CO_2 ratios (~10%) with less SO_2, as occasionally seen during ARIAs, are
more in line with emissions from biomass burning (Andreae and Merlet, 2001; Wang et al., 2010b).

The $\Delta CO/\Delta NO_y$ ratio (equivalent to the slope in a CO vs. NO_y plot) (Fig. 5b) is an indicator for distinguishing plumes with
efficient O_3 formation, Typical values of this ratio are ~40 in background air and between ~4-7 in fresh emissions plumes in
250 Houston (Neuman et al., 2009). The $\Delta CO/\Delta NO_y$ ratio of 14.85 measured during ARIAs indicates some photochemical aging
and contributions from fossil fuel or biomass burning, but high values of CO, NO_y, and SO_2 suggests sampling of air parcels
heavily influenced by power plants. The CO/NO_x emission ratio (Fig. 5c) from ARIAs agrees with higher emission ratios of
gasoline vehicles, while higher amounts of CO, NO_x, and SO_2 indicate coal burning from the residential sector or inefficient
electric generating units. While most of these observations are reflective of the prevalence of low efficiency fossil fuel
255 combustion, the aircraft sampled a plume on June 6 while flying spirals over Julu containing 0.9% CO/CO_2 and 0.4% SO_2/CO_2
(Fig. S3), likely due to a coal-burning power plant operating at high combustion efficiency, either using a sulfur scrubber or
burning low sulfur fuel.

3.2 Observations and sources of VOCs

The total measured VOC mixing ratios ranged from 4 to 23 ppbv, largely dependent upon the altitude of collection, and was
260 mostly dominated by alkanes (Fig. 6). The samples associated with the largest concentrations of O_3 were all collected at
altitudes ~500 m during a period with stagnant high pressure. Generally, the samples collected below 500 m showed larger
amounts of alkenes/alkynes and aromatics than canisters collected elsewhere in the PBL. The top VOCs ranked by mean
volume mixing ratio (Table 3) shows that alkanes dominate the total measured VOC mixing ratio during ARIAs (68%),
followed by alkenes/alkynes (17%), and aromatics (15%). The top 10 VOC species are C2-C5 alkanes, C2-C3 alkenes/alkynes,

265   benzene, and toluene. The observed mixing ratios of ethane and propane are 2.65 ppbv and 1.39 ppbv, respectively, which together accounts for ~52% of the total alkane mixing ratio.

The levels of ambient VOCs during ARIAs are generally lower than prior surface observations since measurements were taken in the PBL away from primary sources. Prior ground-based studies have similarly found alkanes to contribute the majority (>50%) of the total VOC concentration in late spring in the Beijing-Tianjin-Hebei region (Li et al., 2015; Tang et al., 2009;

270   Yuan et al., 2013). The most abundant species during ARIAs are comparable to previous studies finding ethane, propane, and acetylene among the most prevalent, but likely have different sources based on the study location (Jia et al., 2016; Li et al., 2015; Mo et al., 2015; Tang et al., 2009). In the Beijing-Tianjin-Hebei region, ambient acetylene, ethylene, and other light alkanes have been attributed to emissions from gasoline vehicles (Li et al., 2015), while in Guangzhou, the widespread use of LPG has resulted in high levels of propane (Guo et al., 2011). Additionally, our observations have higher amounts of branched

275   alkanes, such as 2,2,4-trimethylpentane and 2-methylheptane, both components of gasoline. Next, we examine the potential sources contributing to observations of VOCs by comparing with ratios and correlations from known sources.

Ethane is the most abundant VOC in this study and correlates well with indicators for biomass and coal burning (R>0.81), such as acetylene, ethylene, benzene, and SO_2. The ratio of acetylene to ethane (Fig. 7a) during ARIAs is 0.59, comparable to the ratio found in a plume of fresh biomass burning in Canada (Blake et al., 1994) and within the range of crop residue burning

280   (~0.2-0.6) found in other studies in China (Chen et al., 2017). High ratios of benzene/propane (1.12) are comparable to dry grass combustion samples collected in the central Pearl River Delta (PRD) (1.6) (Wang et al., 2005) and further confirm the presence of VOCs due to biomass burning.

The C3 and C4 alkanes, including propane and the butanes, are the three main components of LPG and their correlation acts as an indicator for LPG leakage. In this study, a moderate correlation (R~0.50) is found between n-butane and propane and i-

285   butane with n-butane. The ratio of n-butane/propane during ARIAs is 0.60, which agrees well with ratios from vehicle emissions (Liu et al., 2008a), but is lower than slopes measured in the PRD (2.1) (Lai et al., 2009), where VOCs originated from LPG leakage. Additionally, propane correlates well with acetylene and ethylene (Figure 7a), two well-known vehicular emission tracers.

Since acetylene and propane have comparable photochemical lifetimes with respect to OH attack, the ratio can be used to

290   assess the relative importance of fossil fuel combustion and LPG leakage (Goldan et al., 2000). LPG contains propane but not acetylene (acetylene/propane<1) while combustion of fossil fuels commonly produces small amounts of propane relative to acetylene (acetylene/propane>1) (Conner et al., 1995; Gilman et al., 2013; Russo et al., 2010; Watson et al., 2001). In this study, the acetylene/propane ratio (Fig. 7a) is greater than 1, indicating emissions from vehicles (Fraser et al., 1998). These results suggest vehicles are largely responsible for the C3 and C4 alkanes as well as the C2 alkenes/alkynes observations.

295   The C5 alkanes and some C6 alkanes like 2,3-dimethylbutane and 2-methylpentane are found in vehicular exhaust and in gasoline vapor (Tsai et al., 2006). The i-pentane to n-pentane ratio is commonly used to identify the contributions of natural gas, vehicular emissions, and fuel evaporation since these alkanes have similar boiling points, vapor pressures, and reaction

rate coefficients with OH. In areas heavily dominated by natural gas drilling, ratios lie between 0.82-0.89 (Gilman et al., 2013),
while higher ratios are associated with vehicle emissions (2.2-3.8) and fuel evaporation (1.8-4.6) (Jobson et al., 2004;

300 McGaughey et al., 2004; Russo et al., 2010; Wang et al., 2013). In this study, i-pentane and n-pentane are highly correlated
(R=0.93), indicating a common source of these compounds. The slope is 10.3, higher than reported in previous studies in China
(Li et al., 2019), and the large i-pentane concentrations are likely reflective of gasoline evaporation due to the extremely
volatile nature of i-pentane. The influence of fuel evaporative emissions is further identified by strong correlations between
C4-C7 alkanes and alkenes typical of fuel evaporative emissions. Strong correlations of many long-chain alkanes (C6-C7 and

305 octane) with i-pentane (R>0.73 except for cyclohexane) but absence of correlations with acetylene indicates solvent
evaporation may be another source of long-chain alkanes.

Typically, the ratio of cis-2-butene/trans-2-butene is used to determine the source of C4 alkenes (Li et al., 2015; Velasco et al.,
2007). However, in this study, all measurements of cis-2-butene and trans-2-butene are below the detection limit, so assessing
the ratio and correlation is not possible. Previous studies in this region in China have attributed C4 alkenes to vehicular

310 emissions (Li et al., 2015).

The correlation between the C7-C8 aromatics is strong (R>0.76) and revealing of typical signatures from incomplete
combustion. The toluene/ethylbenzene ratio (10.7) is higher than traffic and urban emission ratios (~5-8), but closer to ratios
associated with biomass burning (9.41) (Monod et al., 2001; Parrish et al., 1998). Toluene also correlates with all C7-C9
alkanes (R>0.64) and with i-pentane (R=0.85), compounds from diesel and gasoline evaporation. High levels of toluene

315 reported in Hong Kong by Ho et al., (2004) were suggested to be emitted from gasoline evaporation, while Chan et al., (2006b)
attributed the high toluene levels in different PRD cities to industrial solvent usage.

There is an excellent correlation (R>0.99) between o-xylene and m/p-xylene (Fig. 7b) and the slope (0.33) is comparable to
the emission ratio found in a tunnel study (0.35) (Liu et al., 2008a). The o-xylene/ethylbenzene (0.60, Fig. 7b) slope is lower
than vehicle exhaust emission ratios (1.2-1.8) (Conner et al., 1995; Jobson et al., 2004; Kirchstetter et al., 1996; Rogak et al.,

320 1998; Sagebiel et al., 1996), but the correlation is extremely strong, suggesting the preferential loss of xylenes during transport
due to their higher reactivity. These correlations and ratios suggest incomplete combustion from vehicular emissions and
biomass burning are an important source of C7 and C8 aromatics.

The ratio between benzene/toluene (B/T) is a useful indicator to distinguish between vehicular emissions and other combustion
sources. A ratio ~0.5 is often attributed to vehicular sources (Brocco et al., 1997; Perry and Gee, 1995), while ratios larger

325 than 1 have been reported for coal or charcoal burning (Andreae and Merlet, 2001; Moreira Dos Santos et al., 2004). Benzene
was observed at high mean ratios over Hebei (0.51 ppbv) and the average B/T ratio is 1.8±1.6 ppbv/ppbv. The correlation of
some hydrocarbons can highlight the differences between B/T>1 (N=17) and B/T<1 (N=9). The correlation found between
benzene and acetylene when all samples are grouped together (Fig. 7a) substantially improves just considering "traffic-related"
samples (B/T<1) (R=0.93), suggesting a contribution of vehicular sources to benzene and acetylene measurements.

3.3 The effect of VOCs on ozone formation

In order to effectively reduce O_3 concentrations, it is crucial to understand the relative importance of individual VOCs in terms of the production of O_3 because each VOC exhibits different chemical reactivities. In this section, we present results using the loss rate of each VOC species with OH and ozone formation potential (OFP).

3.3.1 OH loss rate of VOC species

The calculation of the first-order loss rate of OH with different VOCs, termed OH reactivity, provides a measure of the potential to produce HO_2 and RO_2, key intermediate species in the production of O_3 (Stroud et al., 2008). Since the reaction with OH accounts for the majority of loss of most VOCs, the rate constant (obtained from the Master Chemical Mechanism version 3.3.1 (MCM3.3.1) and the National Institute of Standards and Technology (NIST) Chemical Kinetics database (www.kinetics.nist.gov/) for the reaction between OH and various hydrocarbons reflects the overall reactivity of that hydrocarbon (Finlayson-Pitts and Pitts, 1999). OH reactivity for each VOC species (VOC_i) is defined by Equation 2:

$$OHR(VOC_i) = k_{OH+VOC_i} * [VOC_i] \qquad (2)$$

Where k_{OH+VOC_i} is the reaction rate constant between OH and VOC_i. Among the VOC groups, alkanes and alkenes/alkynes both contribute the most to the total VOC reactivity, accounting for 37% each. Aromatics accounted for 26% of the total VOC reactivity. The relative contribution of the top 10 VOCs ranked by mean OH reactivity (Table 4) shows ethylene, propylene, and isoprene among the top measured alkene species, together contributing ~33% to total OH reactivity. Among the alkanes, 2-methylpentane and i-pentane contribute the most (13%) to total OH reactivity, followed by the branched pentanes and propane. Aromatic compounds such as toluene and m/p-xylene constitute 13% to total OH reactivity. Previous ground-based summer studies in China have found larger contributions of isoprene to OH reactivity, ranging from ~10-30% (Li et al., 2015; Xue et al., 2017). Since isoprene is mostly emitted by biogenic sources during the warmer summer months and when soil moisture is sufficient for plant growth, we expect isoprene to have a larger impact on O_3 production in the summer than our study in spring.

3.3.2 Ozone formation potential of NMHCs

Since OH reactivity only provides a qualitative identification of the most reactive species and does not reflect products and their production of further free radicals, we next consider the contribution to the formation of O_3 using ozone formation potential (OFP). The OFP of a VOC relies on the quantity maximum incremental reactivity (MIR), which represents the amount of O_3 formed from the addition of a small amount of the VOC species in interest under high NO_x conditions. Values of MIR (unit: g O_3 formed/ g VOC) have been calculated based on model simulations evaluated with smog chamber measurements (Carter, 2010, 1994). The OFP is calculated according to Equation 3:

$$OFP (VOC_i) = MIR_{VOC_i} * [VOC_i] \qquad (3)$$

360   This method gives an estimate of only the first 24 hours after initial release. The median measured VOC/NO$_x$ ratio for all WAS canisters was 4.9 ppbv/ppbv. In comparison, the ratio of reactive organic gas to NO$_x$ (ROG/NO$_x$) in Los Angeles is 7.6 ppbv/ppbv (Carter, 1994). VOCs experience photochemical loss from emission sources near the surface to measured aloft concentrations. Estimation of OFP from aircraft observations throughout the PBL indicates how formation of O$_3$ may be different from previous surface studies.

365   To identify the major contributors to O$_3$ formation in this region, the 10 species with the highest mean OFP are listed in Table 4. Aromatic compounds are the largest contributor to total OFP (43%), followed by alkanes (30%) and alkenes/alkynes (27%). Toluene and ethylene make the largest contributions (19.6% and 15.7%, respectively) to total OFP. The high MIR of these compounds (MIR=4.0 g O$_3$/g VOC and 9.00 g O$_3$/g VOC, respectively) and large mixing ratios (4.9% and 5.7% of the total measured VOC volume mixing ratio) drives their important contribution to O$_3$ formation. The relatively short lifetime of

370   ethylene (~1.4 days) combined with the large range of measured mixing ratios (0.18 to 3.54 ppbv) suggests sampling of air masses with little to moderate photochemical processing, indicating the large range of influence on OFP. The most reactive compound in terms of OFP is trans-2-butene (MIR=15.16 g O$_3$/g VOC), but its low concentration results in only 0.2% to total OFP. At the other extreme, ethane accounts for a relatively high percentage of total measured VOC volume mixing ratio (17.0%) yet only contributes 2.1% to OFP due to its low reactivity (MIR=0.49 g O$_3$/g VOC).

375   Previous studies in China report aromatics and alkenes account for the most OFP (Cai et al., 2010; Cheng et al., 2010; Jia et al., 2016; Liang et al., 2017; Wang et al., 2010a, 2016; Xie et al., 2008; Zheng et al., 2009). In particular, ethylene, isoprene, toluene, propylene, and m/p-xylene are most influential to OFP at a surface site in Quzhou in June and July 2014 (Li et al., 2015). J. H. Tang et al. (2007) concluded ethylene, toluene, and m/p-xylene are the main contributors to OFP during spring 2005 at the surface in the PRD, citing emissions from industry and vehicular exhaust. Our study agrees with past research in

380   urban areas in China identifying the most reactive VOCs in terms of OFP; O$_3$ appears to be formed more slowly above the surface and in nonurban areas, but production is still substantial.

The current VOC abatement policy in China mainly focuses on the reduction of anthropogenic VOCs from sources in the petrochemical industry, organic chemical industry, packaging printing, and industrial coating, not considering reactivity or chemical speciation (Li et al., 2018). A 2010 VOC emission inventory study concluded the top 15 OFP species (including m/p-

385   xylene, toluene, propylene, o-xylene, and ethylbenzene) contributed 69% of total OFP, but only accounted for 30% of the total emission of VOCs by mass (Liang et al., 2017). Our analysis of the top 10 species ranked by mean OFP shows these compounds contribute 68% to total OFP but only represent 37% of the total volume mixing ratio. Li et al., (2018) classifies industrial coal burning, biomass burning, and motorcycles to the top three VOC emission sources in Shijiazhuang, but OFP is highest for furniture coating, automobile coating, diesel vehicles, fuel evaporation, and gasoline vehicles. These results confirm that

390   reactivity scales and emissions rates should be considered together when formulating control strategies for O$_3$.

3.4 Photochemical ozone production rate and sensitivity

In this section, we describe calculated net photochemical production rates of O_3 using the box model constrained by aircraft observations. Ozone production rates calculated from the box model are high in major urban centres, particularly Shijiazhuang and Xingtai, but also between these cities (Fig. 8a). The highest rates (>10 ppbv/hour) are generally found closer to the surface, but in some instances upwards of 2000 m. The largest net production rate of O_3 (over 16 ppbv/hour) was located along the Taihang Mountains between Shijiazhuang and Xingtai. This large net production rate occurred ~2000 m on June 11, 2016 when NO, NO_y, NO_2, and O_3 were ~2 ppbv, ~18 ppbv, ~3 ppbv, and ~75 ppbv, respectively.

Vertical profiles of production, loss, and net rates of O_3 (Fig. 9) show that HO_2+NO made more O_3 than RO_2+NO during the campaign. The major loss of O_3 was due to the termination of NO_2 through its reaction with OH below 2500 m. Reaction with $O(^1D)$ is the main loss of O_3 above 2500 m. A maximum of net O_3 production for the mean profile was observed in the lowest 500 m of ~7 ppbv/hour. In the PBL between 1500-2000 m, where median NO and NO_2 were 534 and 625 pptv, respectively, O_3 production rates were ~4 ppbv/hour. In the lower FT from 2500 to 3000 m, peak net O_3 production rates still reached ~3ppbv/hour and were conducive to long-range transport.

Values of L_N/Q (Fig. 8b) indicate production rates of O_3 are mostly NO_x-sensitive (i.e., $L_N/Q < 0.5$) in the PBL over Hebei and some of the largest net production rates of O_3 are associated with NO_x-sensitivity. In order to control aloft O_3 production that has the potential to be transported downwind, NO_x is the most important precursor to control. However, at low altitudes near urban centres, the production rate of O_3 tends to be more VOC-sensitive (i.e., $L_N/Q > 0.5$), particularly during morning flights. In Beijing, P. Chen et al., (2013) found a transition of O_3 formation from VOC-limited to NO_x-limited at ~1 km and many studies conclude O_3 production in urban areas of China is VOC-sensitive in spring, while likely more NO_x-sensitive in more rural areas (Ran et al., 2011; Xue et al., 2013). Pusede et al., (2014) assessed the temperature dependence of emission control scenarios to lower O_3 in San Joaquin Valley, California and concluded reducing organic emissions at moderate and high temperatures with co-occurring NO_x decreases will further diminish the number of O_3 violations. Thus, the control of NO_x as well as VOCs may be necessary to control both aloft and near-ground O_3 production in the NCP.

4 Summary

High concentrations of O_3 and its precursors were pervasive over Hebei Province, China in Spring 2016. In this study, we quantify the composition and photochemical nature of the lower troposphere associated with smog events. Measurements of trace gases including O_3, CO, NO_x, NO_y, and of aerosol optical properties were acquired in May and June 2016. Twenty-six samples analysed for 54 VOCs were taken aboard a Y-12 research aircraft mostly in the PBL. Our observations confirm heavy loadings of pollution over Hebei.

The major conclusions of our study are:

1. We observed high amounts O$_3$, ranging from 52 ppbv to 142 ppbv, with the highest values found over Shijiazhuang. The highest NO$_x$ concentrations were observed over Xingtai below 500 m. The NO$_x$ and CO concentrations ranged from 0.15 ppbv to 49 ppbv and from 91 ppbv to about 2,000 ppbv, respectively. Ratios of CO/CO$_2$ and CO/NO$_y$ indicate inefficient combustion from residential coal and biomass burning throughout the region.

2. Concentrations of total measured VOCs reveals alkanes contribute the most by volume mixing ratio (68%), while alkenes/alkynes and aromatics together supply the most (74%) to the calculated OH loss rate. Aromatics constitute most (43%) to the total calculated OFP and toluene, ethylene, m/p-xylene, propylene, and i-pentane play significant roles in the aloft formation of O$_3$ in this region. Sources of VOCs include vehicular emissions, biomass burning, and fuel and solvent evaporation.

3. High amounts of NO$_x$ and VOCs throughout the PBL over nonurban parts of Hebei Province were found to generate O$_3$ at a peak mean rate of ~7 ppbv/hour below 500 m. The lower free troposphere (from ~2500 to ~3000 m) was also frequently polluted with CO and NO$_2$ averaging ~125 ppbv and ~140 pptv with peak net production rates of O$_3$ ~3 ppbv/hour, allowing for continued formation of O$_3$ as the air mass travels downwind. The O$_3$ production regime is found to be NO$_x$-limited throughout the PBL over Hebei, while more VOC-limited at low altitudes near urban centres.

Our measurements in spring 2016 over Hebei cannot represent all of China or the seasonal variation of O$_3$ photochemistry, but measurements from an airborne platform make a valuable addition to the understanding of one of the most polluted regions in China, and indeed the world. We show that to improve air quality in Hebei Province, both NO$_x$ and VOCs from vehicles and fuel evaporation should be targeted. While VOCs are already targeted for emission reduction in China, the egregious concentrations of O$_3$ observed in this study further confirm the formation of a reactivity-oriented control strategy is urgent.

Author contributions

The ARIAs campaign was supervised by RD, ZQ, and XR. XR and HH conducted the measurements on board the research aircraft and VOCs were analyzed by MS and SL. A^{2}BC observations were collected by ZL, FW, YW, and FZ. SR helped set up the box model. SB carried out the scientific analysis of the aircraft data and drafted the manuscript with contributions from all co-authors.

References

Al-Saadi, J., Carmichael, G., Crawford, J., Emmons, L., Kim, S., Song, C. K., Chang, L. S., Lee, G., Kim, J. and Park, R.: NASA Contributions to KORUS-AQ: An International Cooperative Air Quality Field Study in Korea., 2015.

An, J., Wang, J., Zhang, Y. and Zhu, B.: Source Apportionment of Volatile Organic Compounds in an Urban Environment at the Yangtze River Delta, China, Arch. Environ. Contam. Toxicol., 72(3), 335–348, doi:10.1007/s00244-017-0371-3, 2017.

Andreae, M. O. and Merlet, P.: Emission of trace gases and aerosols from biomass burning, Global Biogeochem. Cycles, 15(4), 955–966, doi:10.1029/2000GB001382, 2001.

Avnery, S., Mauzerall, D. L., Liu, J. and Horowitz, L. W.: Global crop yield reductions due to surface ozone exposure: 2. Year 2030 potential crop production losses and economic damage under two scenarios of O_3 pollution, Atmos. Environ., 45(13), 2297–2309, doi:10.1016/j.atmosenv.2011.01.002, 2011.

Barletta, B., Meinardi, S., Rowland, F. S., Chan, C. Y., Wang, X., Zou, S., Lo, Y. C. and Blake, D. R.: Volatile organic compounds in 43 Chinese cities, Atmos. Environ., 39(32), 5979–5990, doi:10.1016/j.atmosenv.2005.06.029, 2005.

Bell, M. L., Peng, R. D. and Dominici, F.: The Exposure – Response Curve for Ozone and Risk of Mortality and the Adequacy of Current Ozone Regulations, Environ. Health Perspect., 114(4), 532–536, doi:10.1289/ehp.8816, 2006.

Blake, D. R., Smith, T. W., Chen, T.-Y., Whipple, W. J. and Rowland, F. S.: Effects of biomass burning on summertime nonmethane hydrocarbon concentrations in the Canadian wetlands, J. Geophys. Res., 99(D1), 1699, doi:10.1029/93jd02598, 1994.

Brocco, D., Fratarcangeli, R., Lepore, L., Petricca, M. and Ventrone, I.: Determination of aromatic hydrocarbons in urban air of Rome, Atmos. Environ., 31(4), 557–566, doi:10.1016/S1352-2310(96)00226-9, 1997.

Cai, C. J., Geng, F. H., Tie, X. X., Yu, Q., Peng, L. and Zhou, G. Q.: Characteristics of ambient volatile organic compounds (VOCs) measured in Shanghai, China, Sensors, 10(8), 7843–7862, doi:10.3390/s100807843, 2010.

Carter, W. P.: Updated Maximum Incremental Reactivity Scale and Hydrocarbon Bin Reactivities for Regulatory Applications., 2010.

Carter, W. P. L.: Development of Ozone Reactivity Scales for Volatile Organic Compounds, Air Waste, 44(7), 881–899, doi:10.1080/1073161X.1994.10467290, 1994.

Chan, L. Y., Chu, K. W., Zou, S. C., Chan, C. Y., Wang, X. M., Barletta, B., Blake, D. R., Guo, H. and Tsai, W. Y.: Characteristics of nonmethane hydrocarbons (NMHCs) in industrial, industrial-urban, and industrial-suburban atmospheres of the Pearl River Delta (PRD) region of south China, J. Geophys. Res. Atmos., 111(11), 1–9, doi:10.1029/2005JD006481, 2006.

Chen, J., Li, C., Ristovski, Z., Milic, A., Gu, Y., Islam, M. S., Wang, S., Hao, J., Zhang, H., He, C., Guo, H., Fu, H., Miljevic, B., Morawska, L., Thai, P., LAM, Y. F., Pereira, G., Ding, A., Huang, X. and Dumka, U. C.: A review of biomass burning: Emissions and impacts on air quality, health and climate in China, Sci. Total Environ., 579(November 2016), 1000–1034, doi:10.1016/j.scitotenv.2016.11.025, 2017.

Chen, P., Quan, J., Zhang, Q., Tie, X., Gao, Y., Li, X. and Huang, M.: Measurements of vertical and horizontal distributions of ozone over Beijing from 2007 to 2010, Atmos. Environ., 74(August), 37–44, doi:10.1016/j.atmosenv.2013.03.026, 2013.

Cheng, H. R., Guo, H., Saunders, S. M., Lam, S. H. M., Jiang, F., Wang, X. M., Simpson, I. J., Blake, D. R., Louie, P. K. K. and Wang, T. J.: Assessing photochemical ozone formation in the Pearl River Delta with a photochemical trajectory model, Atmos. Environ., 44(34), 4199–4208, doi:10.1016/j.atmosenv.2010.07.019, 2010.

Choi, J., Park, R. J., Lee, H., Lee, S., Jo, D. S., Jeong, J. I., Henze, D. K., Woo, J., Ban, S., Lee, M., Lim, C., Park, M., Shin, H. J., Cho, S., Peterson, D. and Song, C.: Impacts of local vs. trans-boundary emissions from different sectors on PM 2.5 exposure in South Korea during the KORUS-AQ campaign, Atmos. Environ., 203, 196–205, doi:10.1016/j.atmosenv.2019.02.008, 2019.

Conner, T. L., Lonneman, W. A. and Seila, R. L.: Transportation-related volatile hydrocarbon source profiles measured in Atlanta, J. Air

Atmospheric
Chemistry
and Physics
Discussions

Waste Manag. Assoc., 45(5), 383–394, doi:10.1080/10473289.1995.10467370, 1995.

Dickerson, R. R., Li, C., Li, Z., Marufu, L. T., Stehr, J. W., Mcclure, B., Krotkov, N., Chen, H., Wang, P., Xia, X., Ban, X., Gong, F., Yuan,
495   J. and Yang, J.: Aircraft observations of dust and pollutants over northeast China : Insight into the meteorological mechanisms of transport,
J. Geophys. Res., 112, 1–13, doi:10.1029/2007JD008999, 2007.

Ding, A. J., Wang, T., Thouret, V., Cammas, J.-P. and Nédélec, P.: Tropospheric ozone climatology over Beijing: analysis of aircraft data
from the MOZAIC program, Atmos. Chem. Phys., 8(1), 1–13, doi:10.5194/acp-8-1-2008, 2008.

Environmental Protection Agency - Integrated Risk Information System: Integrated Risk Information System (IRIS) Chemical Assessment
500   Summary: Benzene ; CASRN 71-43-2., 2003.

Finlayson-Pitts, B. J. and Pitts, J. N.: Chemistry of the Upper and Lower Atmosphere, Academic Press, San Diego, CA., 1999.

Fraser, M. P., Cass, G. R. and Simoneit, B. R. T.: Gas-phase and particle-phase organic compounds emitted from motor vehicle traffic in a
Los Angeles roadway tunnel, Environ. Sci. Technol., 32(14), 2051–2060, doi:10.1021/es970916e, 1998.

Geng, F., Zhang, Q., Tie, X., Huang, M., Ma, X. and Deng, Z.: Aircraft measurements of O_3, NO_x, CO, VOCs, and SO_2 in the Yangtze River
505   Delta region, Atmos. Environ., 43(3), 584–593, doi:10.1016/j.atmosenv.2008.10.021, 2009.

Gilman, J. B., Lerner, B. M., Kuster, W. C. and De Gouw, J. A.: Source signature of volatile organic compounds from oil and natural gas
operations in northeastern Colorado, Environ. Sci. Technol., 47(3), 1297–1305, doi:10.1021/es304119a, 2013.

Goldan, P. D., Parrish, D. D., Kuster, W. C., Trainer, M., McKeen, S. A., Holloway, J., Jobson, B. T., Sueper, D. T. and Fehsenfeld, F. C.:
Airborne measurements of isoprene, CO, and anthropogenic hydrocarbons and their implications, J. Geophys. Res. Atmos., 105(D7), 9091–
510   9105, doi:10.1029/1999JD900429, 2000.

Guo, S., Tan, J., Ma, Y., Yang, F., Yu, Y. and Wang, J.: Characteristics of atmospheric non-methane hydrocarbons during high PM10
episodes and normal days in Foshan, China, Atmos. Res., 101(3), 701–710, doi:10.1016/j.atmosres.2011.04.022, 2011.

Halliday, H. S., Digangi, J. P., Choi, Y., Diskin, G. S., Pusede, S. E. and Rana, M.: Using Short - Term CO/CO_2 Ratios to Assess Air Mass
Differences over the Korean Peninsula during KORUS - AQ, J. Geophys. Res. Atmos., 0–2, doi:10.1029/2018JD029697, 2019.

515   Hatakeyama, S., Takami, A., Wang, W. and Tang, D.: Aerial observation of air pollutants and aerosols over Bo Hai, China, Atmos. Environ.,
39(32), 5893–5898, doi:10.1016/j.atmosenv.2005.06.025, 2005.

He, H., Li, C., Loughner, C. P., Li, Z., Krotkov, N. A., Yang, K., Wang, L., Zheng, Y., Bao, X., Zhao, G. and Dickerson, R. R.: SO_2 over
central China: Measurements, numerical simulations and the tropospheric sulfur budget, J. Geophys. Res., 117, 1–15,
doi:10.1029/2011JD016473, 2012.

520   Ho, K. F., Lee, S. C., Guo, H. and Tsai, W. Y.: Seasonal and diurnal variations of volatile organic compounds (VOCs) in the atmosphere of
Hong Kong, Sci. Total Environ., 322(1–3), 155–166, doi:10.1016/j.scitotenv.2003.10.004, 2004.

Inomata, Y., Iwasaka, Y., Osada, K., Hayashi, M., Mori, I., Kido, M., Hara, K. and Sakai, T.: Vertical distributions of particles and sulfur
gases (volatile sulfur compounds and SO2) over East Asia: Comparison with two aircraft-borne measurements under the Asian continental
outflow in spring and winter, Atmos. Environ., 40(3), 430–444, doi:10.1016/j.atmosenv.2005.09.055, 2006.

525   Jerrett, M., Burnett, R. T., Pope, C. A., Ito, K., Thurston, G., Krewski, D., Shi, Y., Calle, E. and Thun, M.: Long-Term Ozone Exposure and
Mortality, N. Engl. J. Med., 360(11), 1085–1095, doi:10.1056/NEJMoa0803894, 2009.

Jia, C., Mao, X., Huang, T., Liang, X., Wang, Y., Shen, Y., Jiang, W., Wang, H., Bai, Z., Ma, M., Yu, Z., Ma, J. and Gao, H.: Non-methane
hydrocarbons (NMHCs) and their contribution to ozone formation potential in a petrochemical industrialized city, Northwest China, Atmos.
Res., 169, 225–236, doi:10.1016/j.atmosres.2015.10.006, 2016.

530   Jobson, B. T., Berkowitz, C. M., Kuster, W. C., Goldan, P. D., Williams, E. J., Fesenfeld, F. C., Apel, E. C., Karl, T., Lonneman, W. A. and
Riemer, D.: Hydrocarbon source signatures in Houston, Texas: Influence of the petrochemical industry, J. Geophys. Res. D Atmos., 109(24),

1–26, doi:10.1029/2004JD004887, 2004.

Johnson, D., Utembe, S. R. and Jenkin, M. E.: Simulating the detailed chemical composition of secondary organic aerosol formed on a regional scale during the TORCH 2003 campaign in the southern UK, Atmos. Chem. Phys., 6(2), 419–431, doi:10.5194/acp-6-419-2006, 535   2006.

Kirchstetter, T. W., Singer, B. C., Harley, R. A., Kendall, G. R. and Ghan, W.: Impact of oxygenated gasoline use on California light-duty vehicle emissions, Environ. Sci. Technol., 30(2), 661–670, doi:10.1021/es950406p, 1996.

Kleinman, L.: A comparative study of ozone production in five U.S. metropolitan areas, J. Geophys. Res., 110(D2), D02301, doi:10.1029/2004JD005096, 2005a.

540   Kleinman, L.: The dependence of tropospheric ozone production rate on ozone precursors, Atmos. Environ., 39(3), 575–586, doi:10.1016/j.atmosenv.2004.08.047, 2005b.

Krotkov, N. A., McLinden, C. A., Li, C., Lamsal, L. N., Celarier, E. A., Marchenko, S. V., Swartz, W. H., Bucsela, E. J., Joiner, J., Duncan, B. N., Folkert Boersma, K., Pepijn Veefkind, J., Levelt, P. F., Fioletov, V. E., Dickerson, R. R., He, H., Lu, Z. and Streets, D. G.: Aura OMI observations of regional SO₂ and NO₂ pollution changes from 2005 to 2015, Atmos. Chem. Phys., 16(7), 4605–4629, doi:10.5194/acp-16- 545   4605-2016, 2016.

Lai, C. H., Chang, C. C., Wang, C. H., Shao, M., Zhang, Y. and Wang, J. L.: Emissions of liquefied petroleum gas (LPG) from motor vehicles, Atmos. Environ., 43(7), 1456–1463, doi:10.1016/j.atmosenv.2008.11.045, 2009.

Lan, Q., Zhang, L., Li, G., Vermeulen, R., Weinberg, R. S., Dosemeci, M., Rappaport, S. M., Shen, M., Alter, B. P., Wu, Y., Kopp, W., Waidyanatha, S., Rabkin, C., Guo, W., Chanock, S., Hayes, R. B., Linet, M., Kim, S., Yin, S., Rothman, N. and Smith, M. T.: Hematotoxicity 550   in Workers Exposed to Low Levels of Benzene, Science (80-.)., 306(5702), 1774–1776, doi:10.1126/science.1102443, 2004.

Li, B., Sai, S., Ho, H., Gong, S., Ni, J., Li, H., Han, L., Yang, Y. and Qi, Y.: Characterization of VOCs and their related atmospheric processes in a central Chinese city during severe ozone pollution periods, Atmos. Chem. Phys., 617–638, 2019.

Li, C., Krotkov, N. A., Dickerson, R. R., Li, Z., Yang, K. and Chin, M.: Transport and evolution of a pollution plume from northern China: A satellite-based case study, J. Geophys. Res., 115, D00K03, doi:10.1029/2009JD012245, 2010.

555   Li, C., McLinden, C., Fioletov, V., Krotkov, N., Carn, S., Joiner, J., Streets, D., He, H., Ren, X., Li, Z. and Dickerson, R. R.: India Is Overtaking China as the World's Largest Emitter of Anthropogenic Sulfur Dioxide, Sci. Rep., 7(1), 14304, doi:10.1038/s41598-017-14639-8, 2017.

Li, G., Wei, W., Shao, X., Nie, L., Wang, H., Yan, X. and Zhang, R.: A comprehensive classification method for VOC emission sources to tackle air pollution based on VOC species reactivity and emission amounts, J. Environ. Sci., 67, 78–88, doi:10.1016/j.jes.2017.08.003, 2018.

560   Li, L., Xie, S., Zeng, L., Wu, R. and Li, J.: Characteristics of volatile organic compounds and their role in ground-level ozone formation in the Beijing-Tianjin-Hebei region, China, Atmos. Environ., 113, 247–254, doi:10.1016/j.atmosenv.2015.05.021, 2015.

Liang, X., Chen, X., Zhang, J., Shi, T., Sun, X., Fan, L., Wang, L. and Ye, D.: Reactivity-based industrial volatile organic compounds emission inventory and its implications for ozone control strategies in China, Atmos. Environ., 162(2), 115–126, doi:10.1016/j.atmosenv.2017.04.036, 2017.

565   Liu, J. and Si, W.: Using NDVI and air temperature to monitoring winter-wheat phenology in Xingtai, Hebei, China, 2011 Int. Conf. Control. Autom. Syst. Eng. CASE 2011, doi:10.1109/ICCASE.2011.5997798, 2011.

Liu, Y., Shao, M., Fu, L., Lu, S., Zeng, L. and Tang, D.: Source profiles of volatile organic compounds (VOCs) measured in China: Part I, Atmos. Environ., 42(25), 6247–6260, doi:10.1016/j.atmosenv.2008.01.070, 2008a.

Liu, Y., Shao, M., Lu, S., Chang, C., Wang, J. and Chen, G.: Volatile Organic Compound (VOC) measurements in the Pearl River Delta 570   (PRD) region , China, Atmos. Chem. Phys, 8, 1531–1545, 2008b.

17

Long, X., Tie, X., Cao, J., Huang, R., Feng, T., Li, N., Zhao, S., Tian, J., Li, G. and Zhang, Q.: Impact of crop field burning and mountains on heavy haze in the North China Plain: A case study, Atmos. Chem. Phys., 16(15), 9675–9691, doi:10.5194/acp-16-9675-2016, 2016.

Mazzuca, G. M., Ren, X., Loughner, C. P., Estes, M., Crawford, J. H., Pickering, K. E., Weinheimer, A. J. and Dickerson, R. R.: Ozone production and its sensitivity to NO_x and VOCs: Results from the DISCOVER-AQ field experiment, Houston 2013, Atmos. Chem. Phys.,

575   16(22), 14463–14474, doi:10.5194/acp-16-14463-2016, 2016.

McGaughey, G. R., Desai, N. R., Allen, D. T., Seila, R. L., Lonneman, W. A., Fraser, M. P., Harley, R. A., Pollack, A. K., Ivy, J. M. and Price, J. H.: Analysis of motor vehicle emissions in a Houston tunnel during the Texas Air Quality Study 2000, Atmos. Environ., 38(20), 3363–3372, doi:10.1016/j.atmosenv.2004.03.006, 2004.

Mo, Z., Shao, M., Lu, S., Qu, H., Zhou, M., Sun, J. and Gou, B.: Process-specific emission characteristics of volatile organic compounds

580   (VOCs) from petrochemical facilities in the Yangtze River Delta, China, Sci. Total Environ., 533, 422–431, doi:10.1016/j.scitotenv.2015.06.089, 2015.

Monod, A., Sive, B. C., Avino, P., Chen, T., Blake, D. R. and Sherwood Rowland, F.: Monoaromatic compounds in ambient air of various cities: A focus on correlations between the xylenes and ethylbenzene, Atmos. Environ., 35(1), 135–149, doi:10.1016/S1352-2310(00)00274-0, 2001.

585   Moreira Dos Santos, C. Y., De Almeida Azevedo, D. and De Aquino Neto, F. R.: Atmospheric distribution of organic compounds from urban areas near a coal-fired power station, Atmos. Environ., 38(9), 1247–1257, doi:10.1016/j.atmosenv.2003.11.026, 2004.

Neuman, J. A., Nowak, J. B., Zheng, W., Flocke, F., Ryerson, T. B., Trainer, M., Holloway, J. S., Parrish, D. D., Frost, G. J., Peischl, J., Atlas, E. L., Bahreini, R., Wollny, A. G. and Fehsenfeld, F. C.: Relationship between photochemical ozone production and NOx oxidation in Houston, Texas, J. Geophys. Res., 114, D00F08, doi:10.1029/2008JD011688, 2009.

590   Parrish, D. D., Trainer, M., Young, V., Goldan, P. D., Kuster, W. C., Jobson, B. T., Fehsenfeld, F. C., Lonneman, W. A., Zika, R. D., Farmer, C. T., Riemer, D. D. and Rodgers, M. O.: Internal consistency tests for evaluation of measurements of anthropogenic hydrocarbons in the troposphere, J. Geophys. Res. Atmos., 103(D17), 22339–22359, doi:10.1029/98JD01364, 1998.

Perry, R. and Gee, I. L.: Vehicle emissions in relation to fuel composition, Sci. Total Environ., 169(1–3), 149–156, doi:10.1016/0048-9697(95)04643-F, 1995.

595   Pusede, S. E., Gentner, D. R., Wooldridge, P. J., Browne, E. C., Rollins, A. W., Min, K. E., Russell, A. R., Thomas, J., Zhang, L., Brune, W. H., Henry, S. B., Digangi, J. P., Keutsch, F. N., Harrold, S. A., Thornton, J. A., Beaver, M. R., St. Clair, J. M., Wennberg, P. O., Sanders, J., Ren, X., Vandenboer, T. C., Markovic, M. Z., Guha, A., Weber, R., Goldstein, A. H. and Cohen, R. C.: On the temperature dependence of organic reactivity, nitrogen oxides, ozone production, and the impact of emission controls in San Joaquin Valley, California, Atmos. Chem. Phys., 14(7), 3373–3395, doi:10.5194/acp-14-3373-2014, 2014.

600   Ran, L., Zhao, C. S., Xu, W. Y., Lu, X. Q., Han, M., Lin, W. L., Yan, P., Xu, X. B., Deng, Z. Z., Ma, N., Liu, P. F., Yu, J., Liang, W. D. and Chen, L. L.: VOC reactivity and its effect on ozone production during the HaChi summer campaign, Atmos. Chem. Phys., 11(10), 4657–4667, doi:10.5194/acp-11-4657-2011, 2011.

Reich, P. B. and Amundson, R. G.: Ambient levels of ozone reduce net photosynthesis in tree and crop species, Science (80-.)., 230(4725), 566–570, doi:10.1126/science.230.4725.566, 1985.

605   Ren, X., Salmon, O. E., Hansford, J. R., Ahn, D., Hall, D., Benish, S. E., Stratton, P. R., He, H., Sahu, S., Grimes, C., Heimburger, A. M. F., Martin, C. R., Cohen, M. D., Stunder, B., Salawitch, R. J., Ehrman, S. H., Shepson, P. B. and Dickerson, R. R.: Methane Emissions from the Baltimore-Washington Area Based on Airborne Observations: Comparison to Emissions Inventories, J. Geophys. Res. Atmos., 1–14, doi:10.1029/2018JD028851, 2018.

Rogak, S. N., Pott, U., Dann, T. and Wang, D.: Gaseous Emissions from Vehicles in a Traffic Tunnel in Vancouver, British Columbia, J.

610   Air Waste Manag. Assoc., 48(7), 604–615, doi:10.1080/10473289.1998.10463713, 1998.

Russo, R. S., Zhou, Y., White, M. L., Mao, H., Talbot, R. and Sive, B. C.: Multi-year (2004-2008) record of nonmethane hydrocarbons and halocarbons in New England: Seasonal variations and regional sources, Atmos. Chem. Phys., 10(10), 4909–4929, doi:10.5194/acp-10-4909-2010, 2010.

Sagebiel, J. C., Zielinska, B., Pierson, W. R. and Gertler, A. W.: Real-world emissions and calculated reactivities of organic species from
615   motor vehicles, Atmos. Environ., 30(12), 2287–2296, doi:10.1016/1352-2310(95)00117-4, 1996.

Shao, M., Zhang, Y., Zeng, L., Tang, X., Zhang, J., Zhong, L. and Wang, B.: Ground-level ozone in the Pearl River Delta and the roles of VOC and NO_x in its production, J. Environ. Manage., 90(1), 512–518, doi:10.1016/j.jenvman.2007.12.008, 2009.

Sillman, S., Logan, A. and Wofsy, C.: The Sensitivity of Ozone to Nitrogen Oxides and Hydrocarbons in Regional Ozone Episodes, J. Geophys. Res., 95, 1837–1851, 1990.

620   Stavrakou, T., Müller, J., Bauwens, M., Smedt, I. De, Lerot, C. and Roozendael, M. Van: Substantial Underestimation of Post-Harvest Burning Emissions in the North China Plain Revealed by Multi-Species Space Observations, Nat. Publ. Gr., (August), 1–11, doi:10.1038/srep32307, 2016.

Stroud, C. A., Morneau, G., Makar, P. A., Moran, M. D., Gong, W., Pabla, B., Zhang, J., Bouchet, V. S., Fox, D., Venkatesh, S., Wang, D. and Dann, T.: OH-reactivity of volatile organic compounds at urban and rural sites across Canada: Evaluation of air quality model predictions
625   using speciated VOC measurements, Atmos. Environ., 42(33), 7746–7756, doi:10.1016/j.atmosenv.2008.05.054, 2008.

Tang, G., Wang, Y., Li, X., Ji, D., Hsu, S. and Gao, X.: Spatial-temporal variations in surface ozone in Northern China as observed during 2009-2010 and possible implications for future air quality control strategies, Atmos. Chem. Phys., 12(5), 2757–2776, doi:10.5194/acp-12-2757-2012, 2012.

Tang, J. H., Chan, L. Y., Chan, C. Y., Li, Y. S., Chang, C. C., Liu, S. C., Wu, D. and Li, Y. D.: Characteristics and diurnal variations of
630   NMHCs at urban, suburban, and rural sites in the Pearl River Delta and a remote site in South China, Atmos. Environ., 41(38), 8620–8632, doi:10.1016/j.atmosenv.2007.07.029, 2007.

Tang, J. H., Chan, L. Y., Chang, C. C., Liu, S. and Li, Y. S.: Characteristics and sources of non-methane hydrocarbons in background atmospheres of eastern, southwestern, and southern China, J. Geophys. Res. Atmos., 114(3), doi:10.1029/2008JD010333, 2009.

Tsai, W. Y., Chan, L. Y., Blake, D. R. and Chu, K. W.: Vehicular fuel composition and atmospheric emissions in South China: Hong Kong,
635   Macau, Guangzhou, and Zhuhai, Atmos. Chem. Phys., 3281–3288, 2006.

Velasco, E., Lamb, B., Westberg, H., Allwine, E., Sosa, G. and Jobson, B. T.: Distribution , magnitudes , reactivities , ratios and diurnal patterns of volatile organic compounds in the Valley of Mexico during the MCMA 2002 & 2003 field campaigns, Atmos. Chem. Phys., (x), 329–353, 2007.

Wang, B., Shao, M., Lu, S. H., Yuan, B., Zhao, Y., Wang, M., Zhang, S. Q. and Wu, D.: Variation of ambient non-methane hydrocarbons
640   in Beijing city in summer 2008, Atmos. Chem. Phys, 5911–5923, doi:10.5194/acp-10-5911-2010, 2010a.

Wang, F., Li, Z., Ren, X., Jiang, Q., He, H., Dickerson, R. R., Dong, X. and Lv, F.: Vertical distributions of aerosol optical properties during the spring 2016 ARIAs airborne campaign in the North China Plain, Atmos. Chem. Phys. Discuss., (January), 1–22, doi:10.5194/acp-2017-1021, 2018a.

Wang, G., Cheng, S., Wei, W., Zhou, Y., Yao, S. and Zhang, H.: Characteristics and source apportionment of VOCs in the suburban area of
645   Beijing , China, Atmos. Pollut. Res., 7(4), 711–724, doi:10.1016/j.apr.2016.03.006, 2016.

Wang, M., Shao, M., Lu, S. H., Yang, Y. D. and Chen, W. T.: Evidence of coal combustion contribution to ambient VOCs during winter in Beijing, Chinese Chem. Lett., 24(9), 829–832, doi:10.1016/j.cclet.2013.05.029, 2013.

Wang, T., Guo, H., Blake, D. R., Kwok, Y. H., Simpson, I. J. and Li, Y. S.: Measurements of trace gases in the inflow of South China Sea

background air and outflow of regional pollution at Tai O, Southern China, J. Atmos. Chem., 52(3), 295–317, doi:10.1007/s10874-005-

650 2219-x, 2005.

Wang, W., Ma, J., Hatakeyama, S., Liu, X., Chen, Y., Takami, A., Ren, L. and Geng, C.: Aircraft measurements of vertical ultrafine particles profiles over Northern China coastal areas during dust storms in 2006, Atmos. Environ., 42(22), 5715–5720, doi:10.1016/j.atmosenv.2008.03.042, 2008.

Wang, Y., Munger, J. W., Xu, S., McElroy, M. B., Hao, J., Nielsen, C. P. and Ma, H.: CO2 and its correlation with CO at a rural site near

655 Beijing: Implications for combustion efficiency in China, Atmos. Chem. Phys., 10(18), 8881–8897, doi:10.5194/acp-10-8881-2010, 2010b.

Wang, Y., Li, Z., Zhang, Y., Du, W., Zhang, F., Tan, H., Xu, H., Jin, X., Fan, X., Dong, Z., Wang, Q. and Sun, Y.: Characterization of aerosol hygroscopicity, mixing state, and CCN activity at a suburban site in the central North China Plain, Atmos. Chem. Phys. Discuss., 1–34, doi:10.5194/acp-2017-1100, 2018b.

Wang, Y., Dörner, S., Donner, S., Böhnke, S., Smedt, I. De, Dickerson, R. R., Dong, Z., He, H., Li, Z., Li, Z., Li, D., Liu, D., Ren, X., Theys,

660 N., Wang, Y., Wang, Y., Wang, Z., Xu, H., Xu, J. and Wagner, T.: Vertical profiles of NO₂, SO₂, HONO, HCHO, CHOCHO and aerosols derived from MAX-DOAS measurements at a rural site in the central western North China Plain and their relation to emission sources and effects of regional transport, Atmos. Chem. Phys, (2), 5417–5449, 2019.

Watson, J. G., Chow, J. C. and Fujita, E. M.: Review of volatile organic compound source apportionment by chemical mass balance, Atmos. Environ., 35(9), 1567–1584, doi:10.1016/S1352-2310(00)00461-1, 2001.

665 Wolfe, G. M., Marvin, M. R., Roberts, S. J., Travis, K. R. and Liao, J.: The framework for 0-D atmospheric modeling (F0AM) v3.1, Geosci. Model Dev., 9(9), 3309–3319, doi:10.5194/gmd-9-3309-2016, 2016.

Xia, L., Zhang, G., Liu, L., Li, B., Zhan, M., Kong, P. and Wang, H.: Atmospheric CO2 and CO at Jingdezhen station in central China: Understanding the regional transport and combustion efficiency, Atmos. Environ., 222(July 2019), 117104, doi:10.1016/j.atmosenv.2019.117104, 2020.

670 Xie, X., Shao, M., Liu, Y., Lu, S., Chang, C. C. and Chen, Z. M.: Estimate of initial isoprene contribution to ozone formation potential in Beijing, China, Atmos. Environ., 42(24), 6000–6010, doi:10.1016/j.atmosenv.2008.03.035, 2008.

Xue, L. K., Wang, T., Gao, J., Ding, a. J., Zhou, X. H., Blake, D. R., Wang, X. F., Saunders, S. M., Fan, S. J., Zuo, H. C., Zhang, Q. Z. and Wang, W. X.: Ozone production in four major cities of China: sensitivity to ozone precursors and heterogeneous processes, Atmos. Chem. Phys. Discuss., 13(10), 27243–27285, doi:10.5194/acpd-13-27243-2013, 2013.

675 Xue, Y., Ho, S. S. H., Huang, Y., Li, B., Wang, L., Dai, W., Cao, J. and Lee, S.: Source apportionment of VOCs and their impacts on surface ozone in an industry city of Baoji, Northwestern China, Sci. Rep., doi:10.1038/s41598-017-10631-4, 2017.

Yang, X., Wang, X., Yang, W., Xu, J., Ren, L., He, Y., Liu, B., Bai, Z., Meng, F. and Hu, M.: Aircraft measurements of SO₂, NOₓ, CO, and O₃ over the coastal and offshore area of Yellow Sea of China, Environ. Monit. Assess., 188(9), doi:10.1007/s10661-016-5533-7, 2016.

Yuan, B., Hu, W. W., Shao, M., Wang, M., Chen, W. T., Lu, S. H., Zeng, L. M. and Hu, M.: VOC emissions, evolutions and contributions

680 to SOA formation at a receptor site in eastern China, Atmos. Chem. Phys., 13(17), 8815–8832, doi:10.5194/acp-13-8815-2013, 2013.

Zhang, Q., Yuan, B., Shao, M., Wang, X., Lu, S., Lu, K., Wang, M., Chen, L., Chang, C. C. and Liu, S. C.: Variations of ground-level O₃ and its precursors in Beijing in summertime between 2005 and 2011, Atmos. Chem. Phys., 14(12), 6089–6101, doi:10.5194/acp-14-6089-2014, 2014.

Zheng, J., Shao, M., Che, W., Zhang, L., Zhong, L., Zhang, Y. and Streets, D.: Speciated VOC Emission Inventory and Spatial Patterns of

685 Ozone Formation Potential in the Pearl River Delta , China, Enviromental Sci. Technol., 43(22), 8580–8586, 2009.

Zou, Y., Deng, X. J., Zhu, D., Gong, D. C., Wang, H., Li, F., Tan, H. B., Deng, T., Mai, B. R., Liu, X. T. and Wang, B. G.: Characteristics of 1 year of observational data of VOCs , NOx and O3 at a suburban site in Guangzhou , China, Atmos. Chem. Phys., 15, 6625–6636,

doi:10.5194/acp-15-6625-2015, 2015.

Table 1. Y-12 research aircraft instrumentation during ARIAs.

Variable	Method
Aircraft Position	Global Positioning System (GPS)
Meteorology (Temperature, Relative humidity, Pressure, 2-D Wind)	Cloud water inertial probe (CWIP)
Greenhouse Gases (CO_2/CH_4/CO/H_2O)	Cavity Ring Down Spectroscopy Picarro Model G24201-m
Ozone (O_3)	UV-absorption, TECO 49C
Sulfur dioxide (SO_2)	Pulsed fluorescence, TECO 43C
Nitrogen dioxide (NO_2)	Cavity enhanced absorption spectroscopy, Los Gatos RMT-200 CRDS
NO/NO_y	Chemiluminescence, modified TECO 42C with an external Molybdenum converter at 375°C
Aerosol Scattering, b_{scat} (450, 500, 700, nm)	Nephelometer, TSI Model 3563
Aerosol Absorption, b_{abs} (565 nm)	Particle Soot Absorption Photometer (PSAP)
Black Carbon (370, 470, 520, 590, 660, 880, 950 nm)	Aethalometer, Magee Model AE31
Black Carbon	Single-Particle Soot Photometer (SP2)
VOCs	Grab Canisters, GC-MSD/FID

690

695

700

705

Atmospheric
Chemistry
and Physics
Discussions

Table 2. Aircraft monitoring results (all altitudes mostly in the PBL, 1-minute averages) in comparison with other airborne studies in the region. All units ppbv.

	This Study, ARIAs		KORUS-AQ[*]	Yellow Sea, coastal and offshore[a]		YRD[b]	Northeast China[c]	Northern China[d]	Bohai Sea[e]	Japan Sea[f]
	May-June 2016		May 24-29	April 2011		October 2007	April 5, 2007	April 2006	March 2002	April 1996
ppbv	Ave (STD)	Min/Max	Ave. (STD)	Ave	Min/Max	Min/Max	Ahead of cold front	Ave	Min/Max	Min/Max
NO_x	5.7 (7.9)	0.15/49.3	1.3 (4.9)	2.45	0.49/9.58	3/40	-	5.01	-/18	-/-
CO	275.0 (202.8)	90.6/1981.6	258.2 (144.5)	980	630/1950	3000/7000	~300	-	-/-	-/-
O_3	85.5 (15.6)	51.6/142.5	89.8 (17.5)	76.3	43.0/126.5	20/60	~70	43.8	35/65	70/90

[*] Statistics calculated for 1-second data during three flights at all altitudes during the "extreme pollution period" (Choi et al.,
710 2019) where the KORUS-AQ DC-8 flew over the Yellow Sea to measure outflow from China.
[a] Yang et al., (2016).
[b] Geng et al., (2009).
[c] Dickerson et al., (2007)
[d] Wang et al., (2008).
715 [e] Hatakeyama et al., (2005).
[f] Inomata et al., (2006).

720

725

730

735

740

Atmospheric
Chemistry
and Physics
Discussions

Table 3. Comparison of the top 10 most abundant species measured in this study with other ground observations in China (Units: ppbv).

	This Study			43 Cities[a]	QZ[b]	GZ[d]	FS[e]	LZ[f]	BJ[b]	NJ[c]
	May-June 2016			January-February 2001	July 2014	June 2011-May 2012	December 2008	June 2013-August 2013	May 2014	June-August 2014
	Ave	%	Range	Range	Ave	Ave	Ave	Ave	Ave	Range
Ethane	2.65	17.0	1.80-4.15	3.7-17.0	3.53	3.66	16.91	-	4.37	0.04-19.35
Propane	1.39	8.9	0.98-1.89	1.5-20.8	1.31	4.34	16.26	3.40	2.44	0.20-6.74
Ethylene	0.88	5.7	0.18-3.54	2.1-34.8	1.92	2.99	28.46	-	2.33	0.27-23.68
Acetylene	0.80	5.1	0.23-1.93	2.9-58.3	1.94	-	32.82	-	2.17	0.02-7.96
Toluene	0.76	4.9	0.03-4.40	0.4-11.2	0.48	4.59	18.87	1.01	1.33	0.01-5.40
i-Pentane	0.67	4.3	0.03-5.44	0.3-18.8	0.60	1.72	1.84	2.43	0.99	0.01-4.32
i-Butane	0.62	4.0	0.06-3.96	0.4-4.6	-	2.67	4.66	2.43	1.03	0.01-3.48
Benzene	0.51	3.3	0.06-2.18	0.7-10.4	0.81	0.62	6.00	1.94	0.82	0.02-11.79
2,2,4-Trimethylpentane	0.43	2.8	0.01-5.42	-	-	0.22	-	0.10	-	0.01-0.63
2-Methylheptane	0.40	2.6	0.01-5.52	-	-	0.08	0	1.49	-	0.01-0.46

[a]43 Cities, China (Barletta et al., 2005).
745   [b]QZ, Quzhou, BJ, Beijing (Li et al., 2015).
[c]NJ, Nanjing, Yangtze River Delta (An et al., 2017).
[d]GZ, Guangzhou, Pearl River Delta (Zou et al., 2015).
[e]FS, Foshan, Pearl River Delta, haze days (Guo et al., 2011).
[f]LZ, Lanzhou (Jia et al., 2016).
750

755

760

765

Atmospheric
Chemistry
and Physics
Discussions
Open Access

Table 4. Top 10 VOC species (mean and percentage breakdown) which contribute to ozone formation based on OH reactivity and Ozone formation potential during ARIAs.

770

OH Reactivity			Ozone Formation Potential		
Species	Mean (s^{-1})	%	Species	Mean (ppbv O_3)	%
Ethylene	0.18	15.7	Toluene	5.81	19.6
Propylene	0.11	9.6	Ethylene	4.65	15.7
Toluene	0.10	8.9	m/p-Xylene	1.87	6.3
2-Methylheptane	0.09	7.9	Propylene	1.72	5.8
Isoprene	0.08	7.2	i-Pentane	1.47	5.0
i-Pentane	0.06	5.1	2,2,4-Trimethylpentane	1.30	4.4
m/p-Xylene	0.05	4.1	2-Methylheptane	1.02	3.4
2,3,4-Trimethylpentane	0.03	3.0	i-Butane	0.93	3.1
2,2,4-Trimethylpentane	0.03	2.8	o-Xylene	0.72	2.4
Propane	0.03	2.7	1,2,4-Trimethylbenzene	0.67	2.3

775

780

785
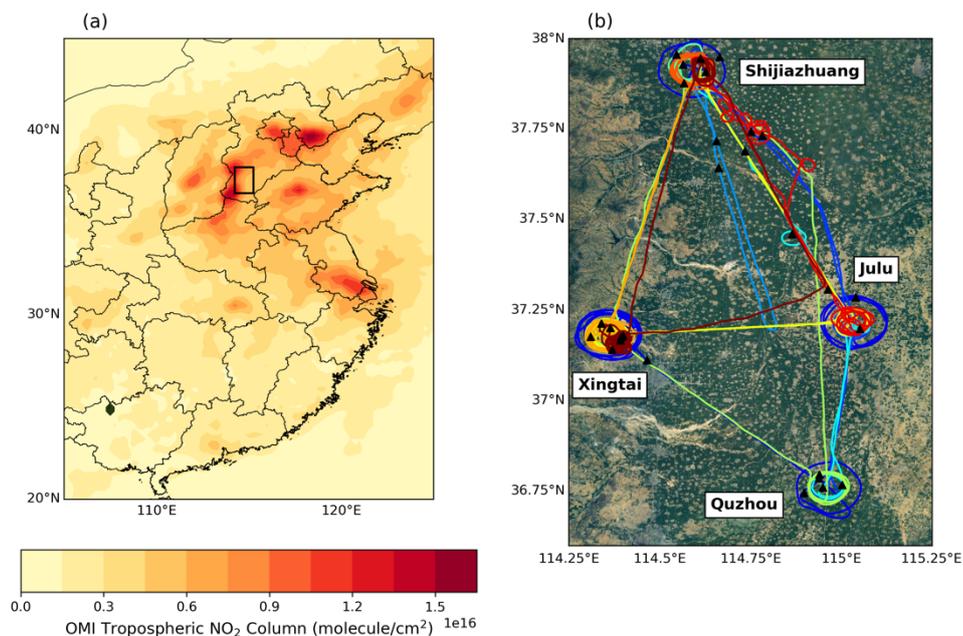
Figure 1. (a) May and June 2016 OMI tropospheric column NO₂ from NASA Goddard Earth Sciences Data and Information Services Centre. The North China Plain is clearly seen in the centre with high column NO₂ concentrations; the black rectangle indicates ARIAs campaign domain and corresponds to the region shown in panel b. (b) Map of 11 ARIAs flight tracks (colored by flight number) and location of VOC samples (black triangles). The background map is provided by Esri, Copyright: ©2009.
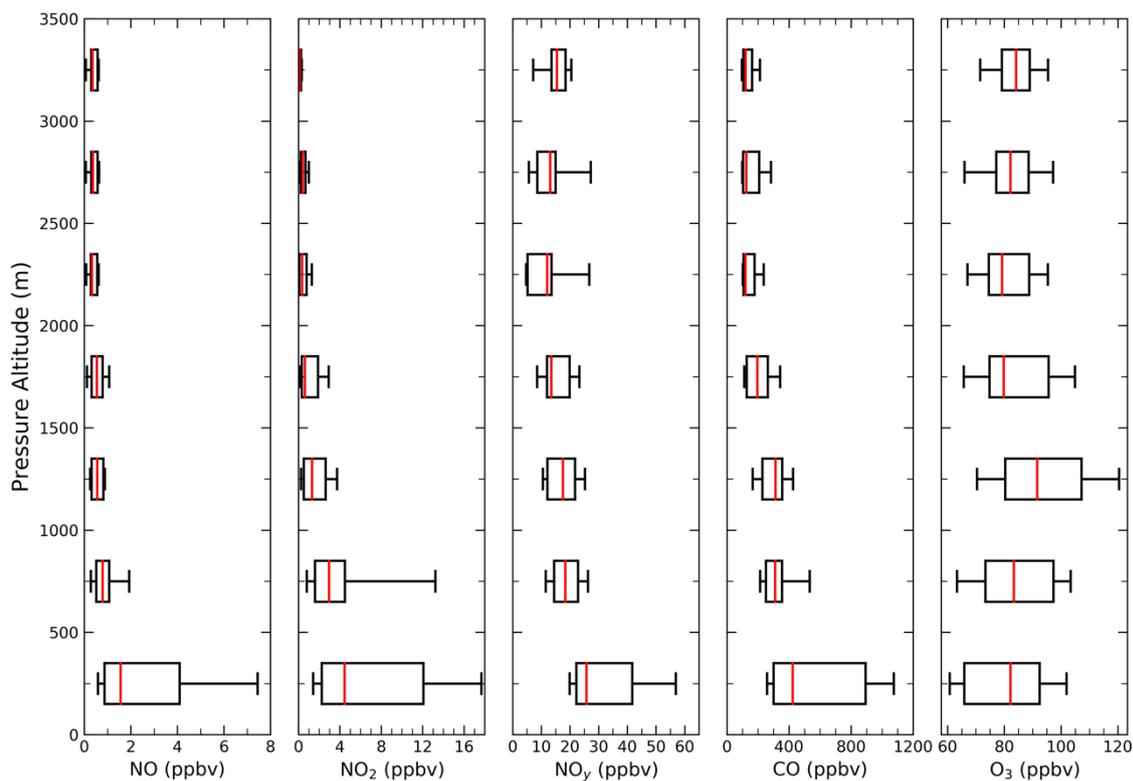
790

Figure 2. Box and whisker plots of 1-second profiles of NO, NO₂, NOy, CO, and O₃ for data collected in 500 m bins. The whiskers show the 10th and 90th percentiles, the box denotes the 25th and 75th percentiles, and the central red line indicates the median value within each bin. Average PBL height for all ARIAs flight is ~1500 m. The total number of observations at altitudes above 2500 m of NO and NOy is small (~2,200 or about ~30 minutes of measurements) since the NO/NOy instrument cannot measure both species simultaneously.

795
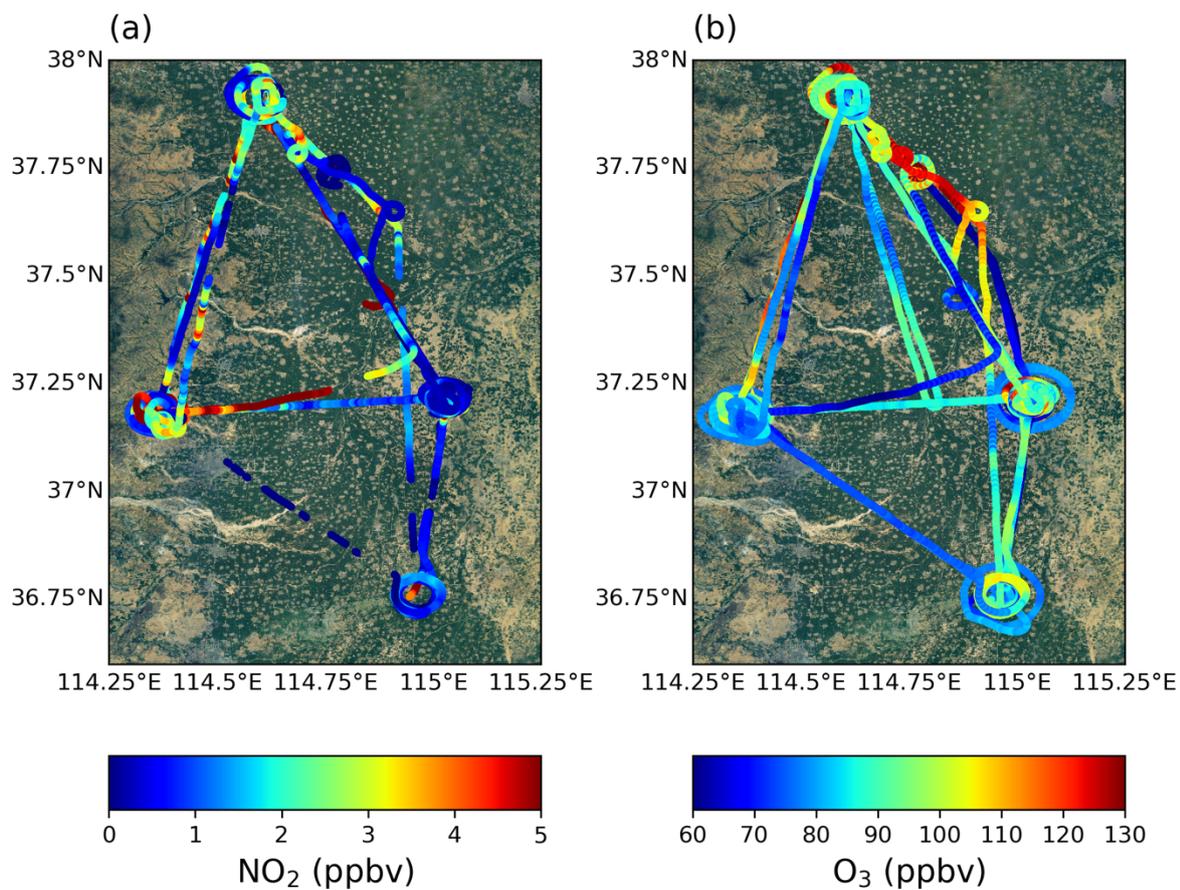
Figure 3. Maps of the ARIAs flight track colored by the 1-second measured mixing ratio (ppbv) of NO$_2$ (a) and O$_3$ (b). The background map is provided by Esri, Copyright: ©2009.

Atmospheric
Chemistry
and Physics
Discussions
Open Access
EGU
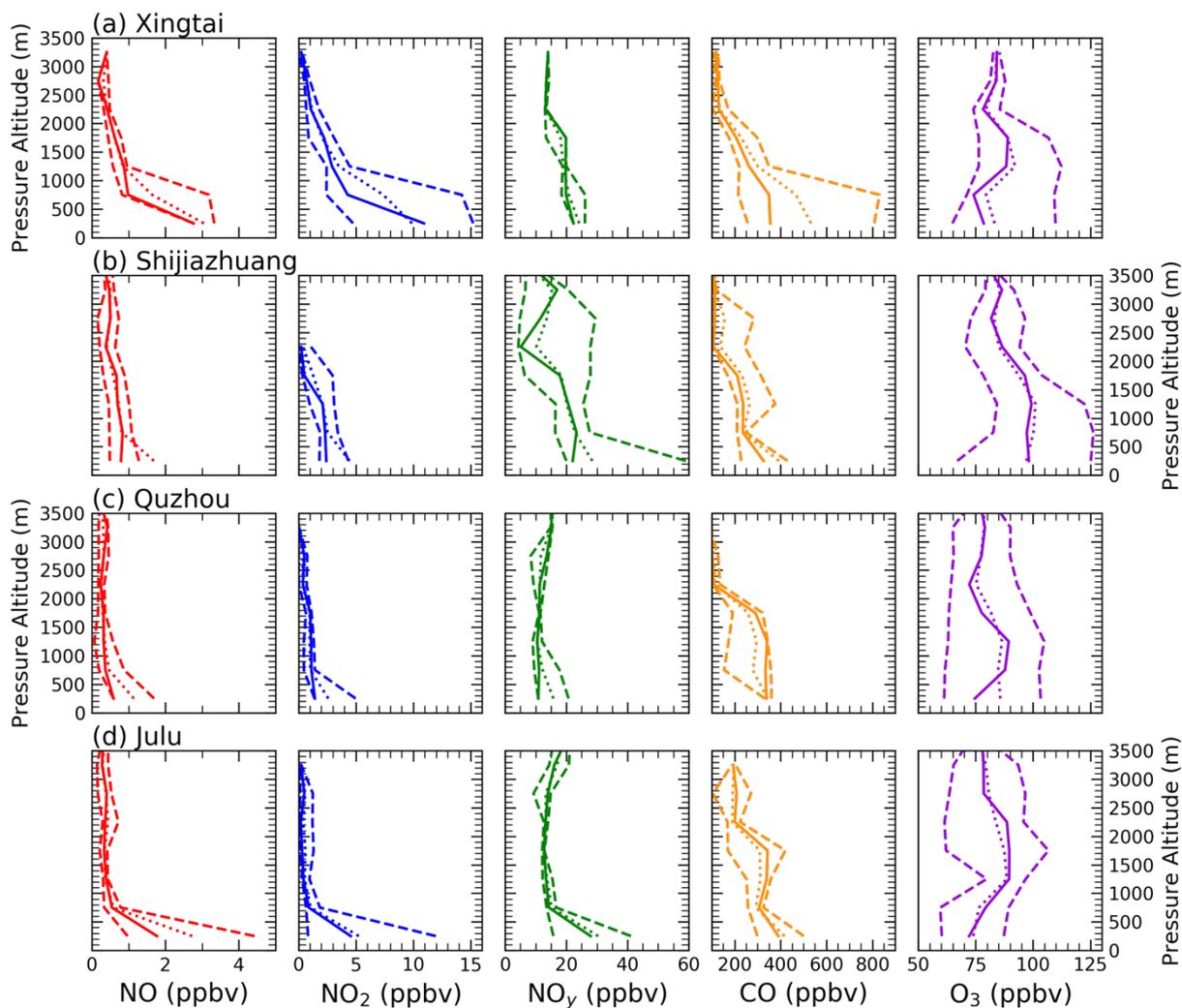
Figure 4. Vertical profiles of 1-second NO (red), NO₂ (blue), NOᵧ (green), CO (orange), and O₃ (purple) in 500 m bins over the 4 spiral locations: Xingtai (a), Shijiazhuang (b), Quzhou (c), and Julu (d). The dashed lines indicate the 10ᵗʰ and 90ᵗʰ percentiles, the solid line is the median and the dotted line is the mean.
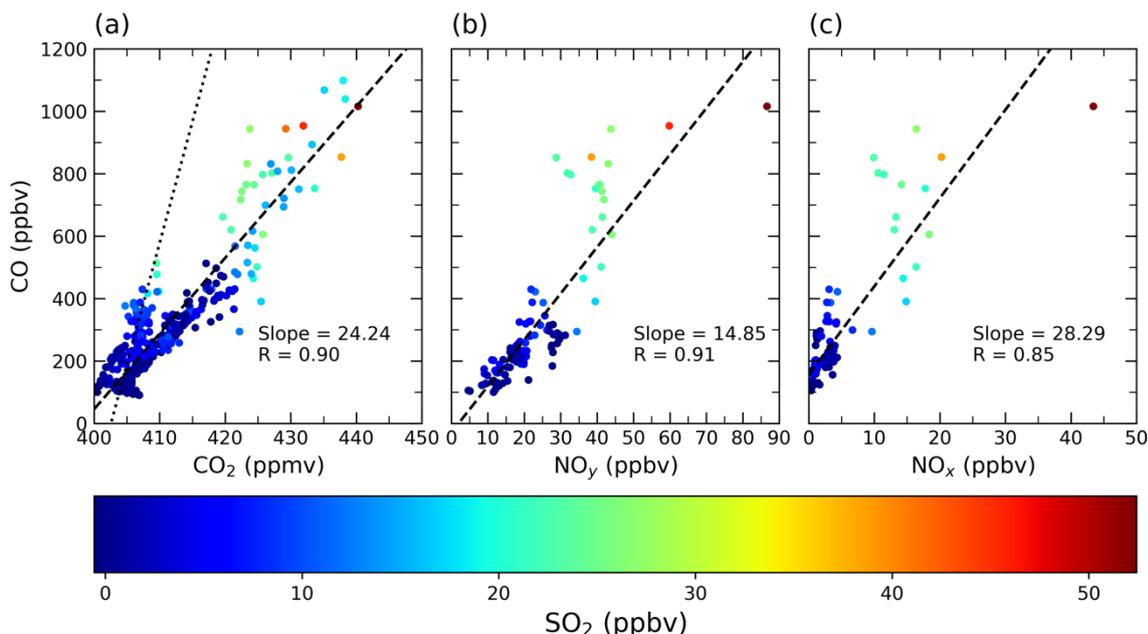
805 **Figure 5. Scatter plots of 1-minute average (a) CO and CO₂, (b) CO and NO_y, and (c) CO and NO_x colored by the SO₂ mixing ratio for all ARIAs flights. The dashed line shows the linear regression for each plot. The dotted line in panel a indicates the higher ratio commonly associated with biomass burning.**
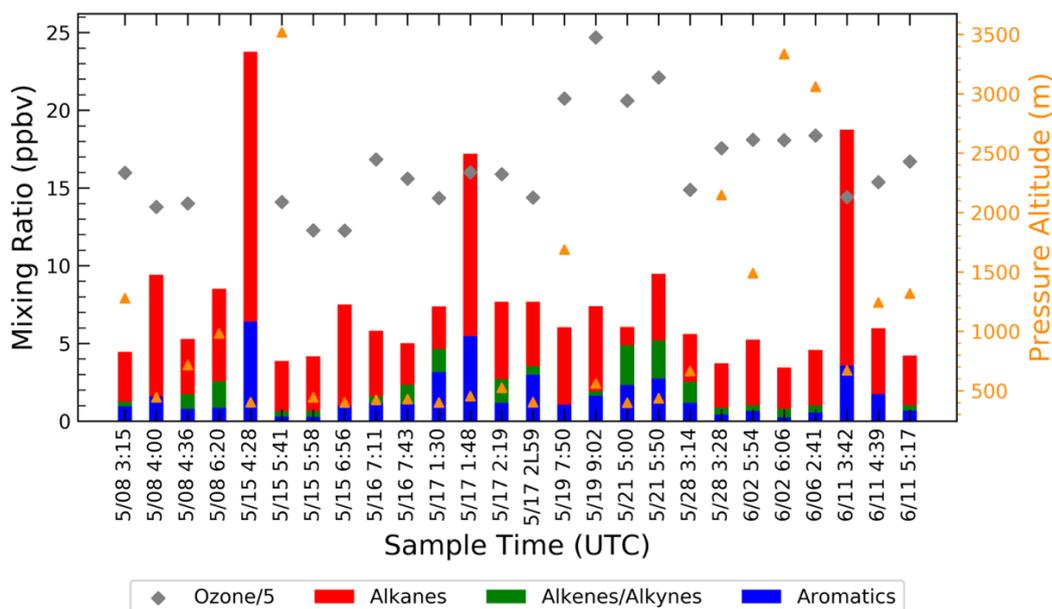
Figure 6. Total VOC mixing ratio for each WAS canister during ARIAs colored by alkanes (red), alkenes/alkynes (green), and aromatics (blue). The concurrent O₃ mixing ratio, divided by 5, is shown in grey diamonds (using left y-axis) and the pressure altitude
810 **of the sample is denoted by orange triangles (using right y-axis).**
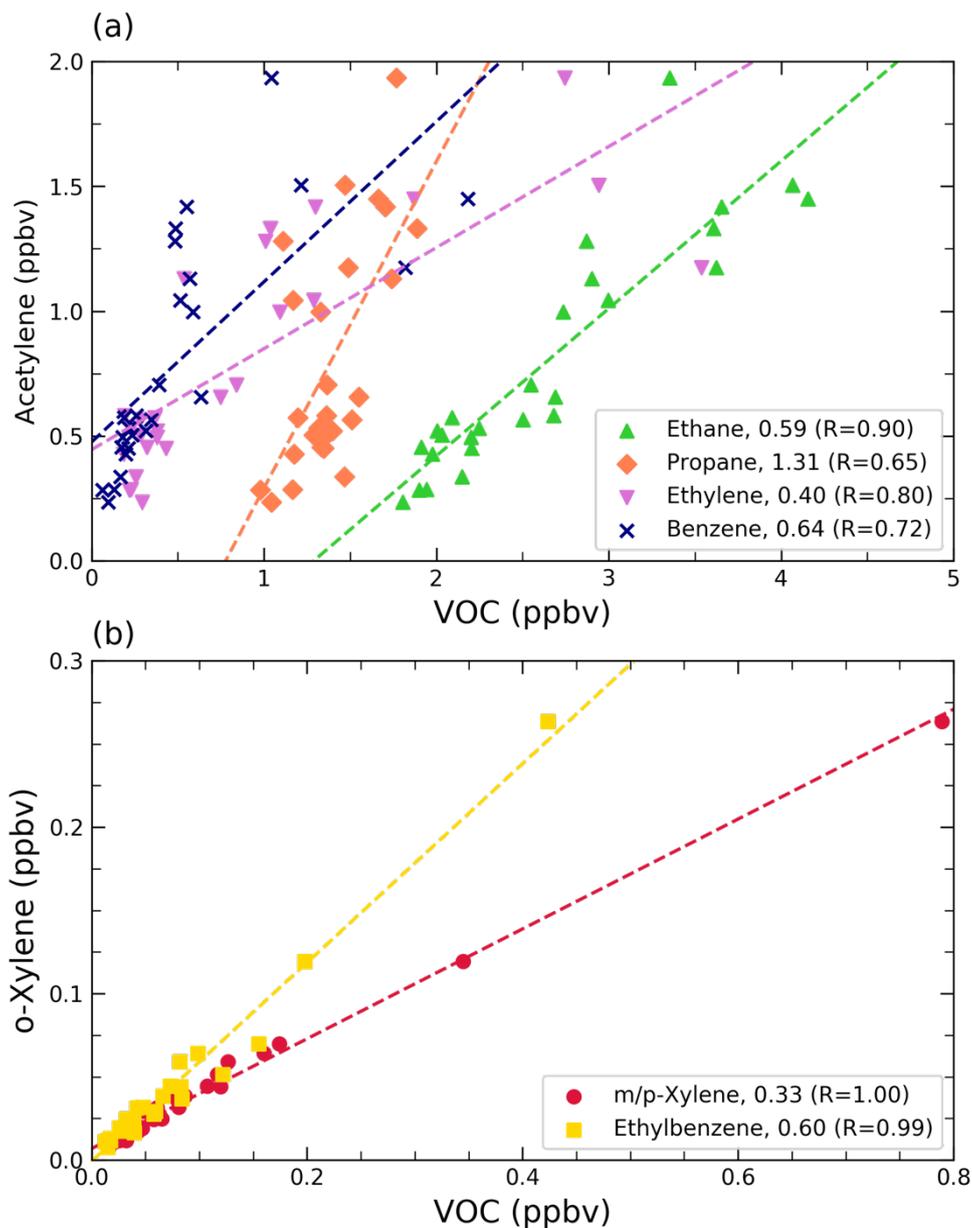
Figure 7. (a) Scatterplot of acetylene with ethane (green upward triangles), propane (orange diamonds), ethylene (purple downward triangles), and benzene (navy ×'s) for all WAS canisters during ARIAs. (b) Regression plots of o-xylene with m/p-xylene (red circles) and ethylbenzene (yellow squares). The dashed lines show the results of a linear least squares regression line for all data points.
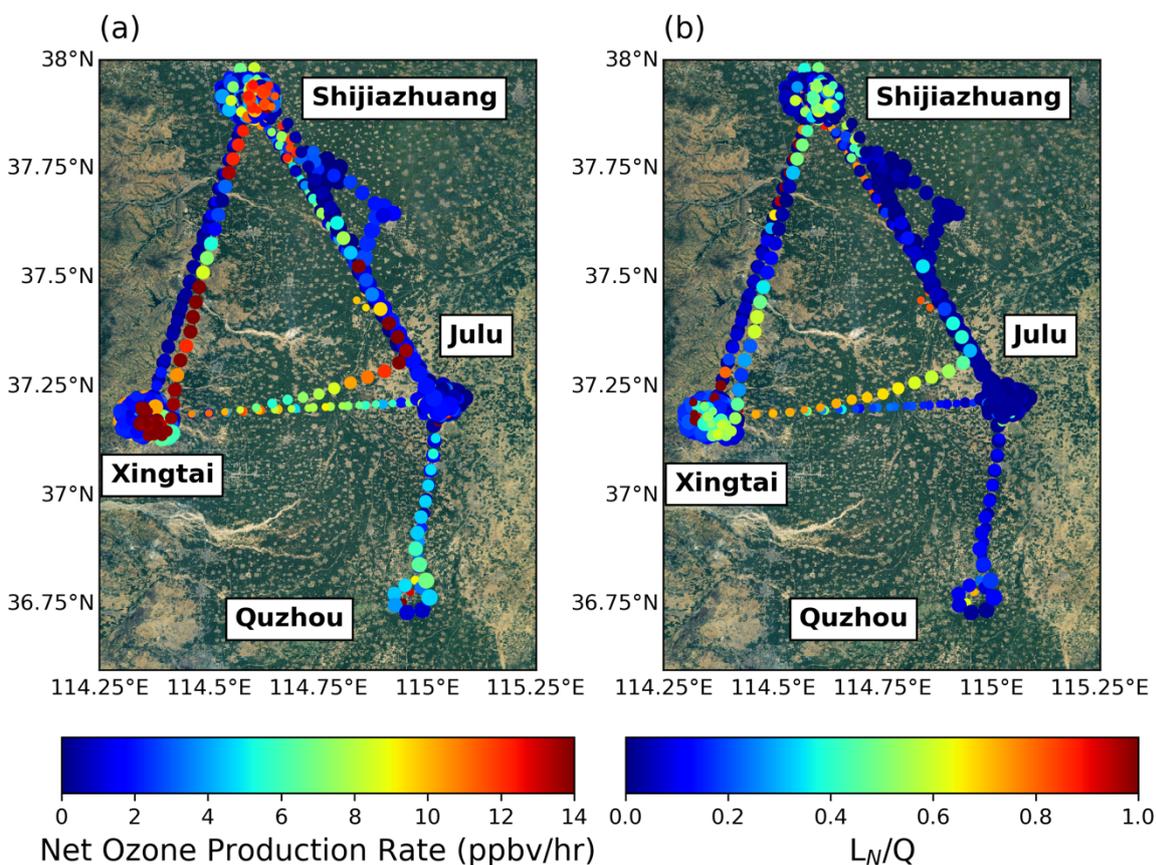
Figure 8. (a) Map of the net production rates of O₃ calculated using F0AM box model results along the Y-12 flight track during ARIAs. (b) Map of L_N/Q, an O₃ sensitivity indicator, along the Y-12 flight path. Ozone production is VOC-sensitive when $L_N/Q > 0.5$ and NOₓ-sensitive when $L_N/Q < 0.5$ (Kleinman, 2005a). The size of the dots in both plots is proportional to the production rate of O₃. The background map is provided by Esri, Copyright: ©2009.
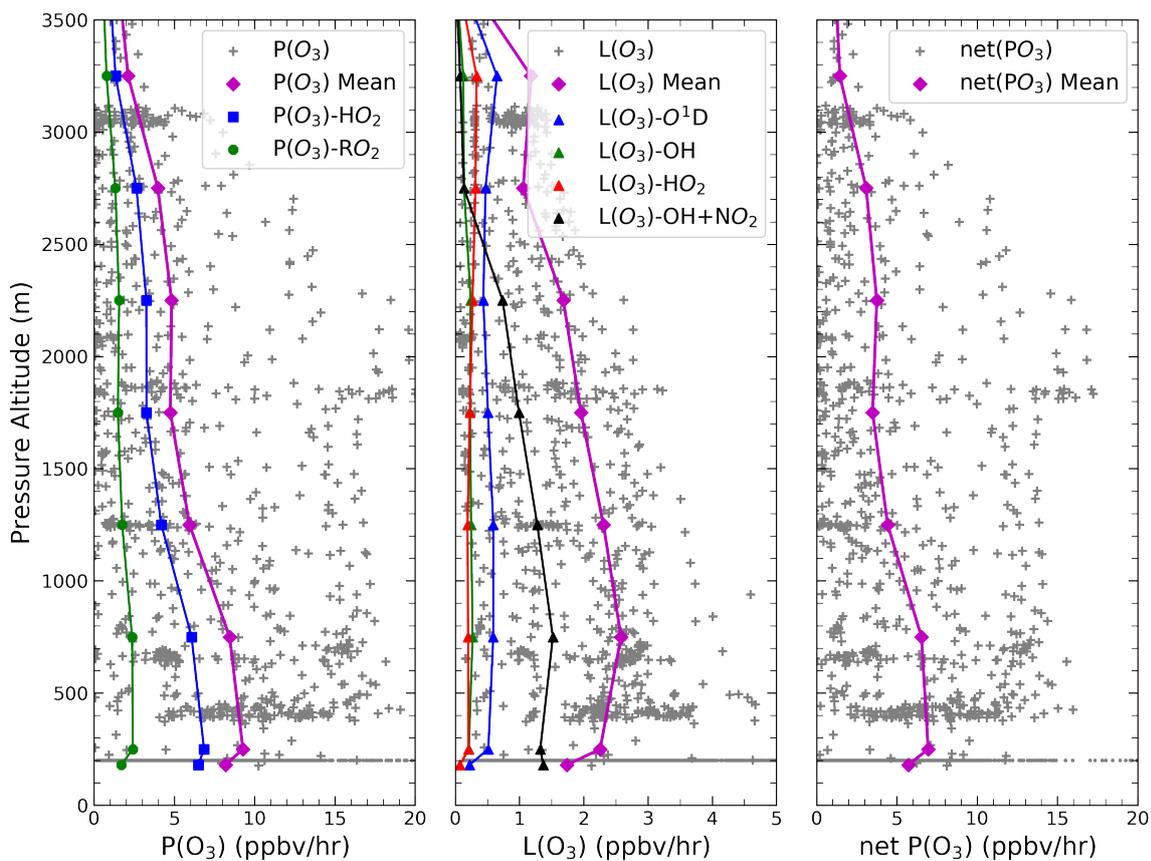
820

Figure 9. Vertical profiles of the rate of production of O₃ (left), O₃ loss rate (middle), and net O₃ production rate (right) during ARIAs.